

Thermodynamic Properties of Octamethylcyclotetrasiloxane

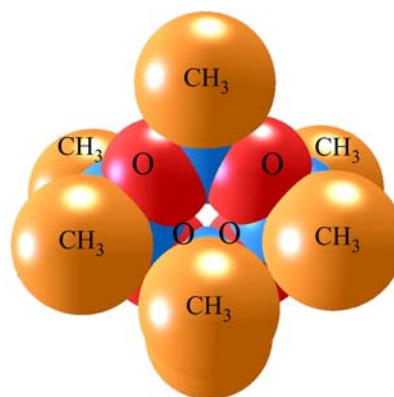
Monika Thol¹, Gabor Rutkai², Andreas Köster², Frithjof H. Dubberke²,
Thorsten Windmann², Roland Span¹, Jadran Vrabec^{2*}

¹Thermodynamics, Ruhr-Universität Bochum, Universitätsstraße 150, 44801 Bochum,
Germany

²Thermodynamics and Energy Technology, Universität Paderborn, Warburger Straße 100,
33098 Paderborn, Germany

E-mail address corresponding author:

jadran.vrabec@uni-paderborn.de



ABSTRACT

An equation of state for octamethylcyclotetrasiloxane is presented. The available experimental data from the literature are supplemented by new measurements on the speed of sound. Furthermore, a new force field is proposed allowing for the generation of a comprehensive thermodynamic data set by means of molecular simulation. Both experimental and molecular simulation data are applied to develop a fundamental equation of state in terms of the Helmholtz energy. Based on the experimental data, the equation of state is valid from the triple point temperature to $T = 590$ K for pressures up to $p = 180$ MPa, and can be used to calculate any thermodynamic state property. Its accuracy is assessed by a comprehensive analysis of the underlying experimental data. Finally, the range of validity was extended to $T_{\max} = 1200$ K and $p_{\max} = 520$ MPa by means of molecular simulation data.

Key words: equation of state, Helmholtz energy, molecular simulation, octamethylcyclotetrasiloxane, speed of sound, thermodynamic properties

1 INTRODUCTION

Octamethylcyclotetrasiloxane (CAS No. 556-67-2, chemical formula $C_8H_{24}O_4Si_4$) is a cyclic siloxane, which is a colorless oily liquid under standard conditions. In the chemical industry, it is used as an adhesive and sealant, as a finishing agent, or a solvent. Furthermore, it is an ingredient of paints, plastics, and rubber products.¹ In the field of energy technology, it is mainly employed as a working fluid in Organic Rankine cycles (ORC) due to some favorable properties, e.g., it is non-toxic, hardly flammable, and chemically stable up to high temperatures.¹ Over the last years, siloxanes were studied comprehensively with the aim to use them in ORC processes. For the design and optimization of such processes, it is essential to have an accurate knowledge of the thermodynamic properties of the fluids involved. The first fundamental equation of state in terms of the Helmholtz energy that provided this information was published by Colonna *et al.*² in 2006. Since the data situation was restricted in terms of quality and quantity at that time, it was challenging to develop a substance specific equation of state for this fluid. Therefore, the generalized functional form for non- and weakly polar fluids of Span and Wagner³ was applied and only the coefficients of the equation of state were fitted to the available experimental data base. Recent investigations showed that the available equation of state exhibits disadvantageous with respect to the speed of sound and density in the homogeneous liquid phase as well as its extrapolation behavior.

In the last decades, several approaches were proposed to overcome the problem of insufficient experimental data for the development of accurate fundamental equations of state, e.g., the construction of generalized functional forms for certain groups of fluids with analogous characteristics.³⁻⁹ A new approach suggested by Rutkai *et al.*¹⁰ comprises the implementation of molecular simulation data in the fitting procedure. Significant progress in computational technology and molecular modeling allow for time efficient and comprehensive simulations of thermodynamic properties. Here, no restrictions due to challenging fluid characteristics, like toxicity and corrosivity, or apparatus limitations with respect to temperature or pressure have to be taken into account. Therefore, these data provide a potential solution to fill gaps in the experimental data base. This new approach was successfully applied to the development of fundamental equations of state for ethylene oxide¹¹ and hexamethyldisiloxane.¹² Following these lines, a potential model for octamethylcyclotetrasiloxane is presented in this work. The available experimental data are complemented by new measurements of the speed of sound in the liquid state. Both experimental and molecular simulation data sets were utilized for the development of the present equation of state.

2 SPEED OF SOUND MEASUREMENT AND MOLECULAR MODELING

The speed of sound of a given fluid can be determined by the time measurement of acoustic signal propagation through the fluid over some known distance. Here, the applied measurement principle is based on estimating the time difference Δt between the detection of two distinct echoes of a signal emitted by a modulated high frequency wave burst with a piezoelectric quartz crystal.^{13,14} In the measurement cell, the crystal is placed between two reflectors that are positioned at distances l_1 and l_2 from the crystal such that $l_1 < l_2$. The reflectors ensure that the echoes of the original signal are also detected with the crystal. The time shift Δt between the detections is caused by the different propagation path lengths l_1 and l_2 . The speed of sound is then given with the ratio of the propagation distances l_1 and l_2 , and with Δt by

$$w = \frac{2(l_2 - l_1)}{\Delta t} \quad (1)$$

assuming that dispersion and diffraction effects can be neglected. The estimation of the time difference Δt was carried out here with the correlation method of Ball and Trusler¹⁵ combined with signal enhancement by fast Fourier transformation. Details of the calculation method and the signal processing are given by Dubberke *et al.*¹⁶

The sample was obtained from WACKER with a given purity of $\geq 99\%$. Before the measurement, the cell was filled with degassed octamethylcyclotetrasiloxane and the fluid was compressed to about 20 MPa by a hand-pump. A constant pressure level was reached after one hour of equilibration. The pressure was measured with a transducer (Honeywell TJE with an operating range up to 70 MPa), calibrated with a dead weight tester (Degranges and Hout, 5201-S) and protected by a blowout disc. The temperature was measured with a Pt100 thermometer (Rössel Messtechnik RM-type), which was installed on the wall of the pressure cylinder next to the quartz crystal and was calibrated with a standardized 25 Ω platinum thermometer (Rosemount 162 CE). The thermostat was constructed with three nested copper shields to allow for fine temperature adjustment of the cell over a wide temperature range. Each shield was equipped with its own independently adjustable heater; each was controlled with a combination of a PID and a proportional (P) controller. For the path length difference Δl , calibration measurements were carried out with water. Water at high purity and accurate speed of sound measurement data are available over a wide range of temperature and pressure. Details are described by Gedanitz *et al.*¹⁷ The obtained speed of sound data were amended by the diffraction correction of Harris,¹⁸ where significant dispersion effects are not expected for a resonance frequency of 8 MHz.¹⁹ The reported uncertainties u_w for the speed of sound were estimated according to the error propagation law, considering the uncertainty of the temperature and pressure measurements as well as the uncertainty of the referencing

procedure. The measurements were carried out along 6 isotherms in the temperature range from 300 K to 550 K up to 26 MPa (54 data points in total). Numerical results are given in the Supplementary Material.

In addition to the speed of sound measurements, molecular simulations were carried out to generate a data set of 6 Helmholtz energy derivatives at 87 state points resulting in a set of 522 thermodynamically non-redundant entries. The calculations were performed with the molecular simulation tool *ms2*²⁰ through the use of the recently implemented formalism of Lustig^{21,22}. This new feature allows for the calculation of the residual part A_{nm}^r of the derivatives

$$\frac{\partial^{n+m} a(T, \rho) / (RT)}{\partial (1/T)^n \partial \rho^m} (1/T)^n \rho^m \equiv A_{nm} = A_{nm}^o + A_{nm}^r \quad (2)$$

for any $n > 0$ or $m > 0$ per sampled state point, where a is the molar Helmholtz energy, T the temperature, ρ the density, and $R = 8.3144621 \text{ J}\cdot\text{mol}^{-1}\cdot\text{K}^{-1}$ ²³ is the universal gas constant. The ideal part $A_{00}^o = A_{00}^o(T) + \ln(\rho/\rho_{\text{ref}})$, with ρ_{ref} being an arbitrary reference density,²⁴ corresponds to the value of $A_{00}^o(T, \rho)$ when no intermolecular interaction are present. Consequently, $A_{00}^o = 0$ for $n > 0$ and $m > 0$, and $A_{00}^o = (-1)^{1+m}$ for $n = 0$ and $m > 0$. $A_{00}^o(T)$ has non-trivial but exclusive temperature dependence and it is a sum of contributions due to translational, rotational, and internal molecular degrees of freedom. Since $a/(RT)$ is a thermodynamic potential, every other equilibrium thermodynamic property can be obtained as a combination of A_{nm} derivatives. Examples are given later on (Eqs. (12) to (15)). A more complete list is given by Span.²⁴

The quality of molecular simulation results is predominantly dependent on the underlying molecular interaction model. The octamethylcyclotetrasiloxane model developed in this work consists of 16 Lennard-Jones (LJ) sites and eight point charges, cf. Figure 1. The geometry of the model was determined by quantum chemical calculations applying the software package GAMESS(US)²⁵ with the Hartree-Fock method and the 6-31G basis set. The initial values of the LJ energy (ϵ) and size (σ) parameters as well as those of the point charges (q) were adopted from Thol *et al.*¹² In the initial phase, the magnitudes of the point charges were adjusted to experimental vapor-liquid equilibrium data, namely saturated liquid density and vapor pressure data. In the last step, all model parameters, including geometric structure, were fine-tuned with the reduced unit method.²⁶ The resulting model parameters are listed in Table 1. The model itself considers no internal degrees of freedom, which can be justified by the compact structure of the model. Therefore, the terms A_{nm}^o were represented by the EOS presented here for the calculation of the ideal contribution in thermodynamic properties for which this contribution is necessary, cf. Eqs. (12), (14), and (15). Finally, the model was validated by comparing simulation results with experimental vapor-liquid equilibrium data as well as single phase liquid density, speed of sound, second virial coefficient, and transport

property data from the literature. Numerical simulation results and comparisons with the new equation of state are given in the Supporting Information. The molecular force field model by Matsubara *et al.*²⁷ is similar in terms of the united-atom approach and rigid body approximation. Although it leads to excellent results for transport properties, the representation of the pressure-volume-density (pVT) relation is inferior. Recently, Xu and Leng²⁸ published a new model for octamethylcyclotetrasiloxane, which is better suited for pVT data, considering the internal molecular degrees of freedom. The performance of the molecular model for the speed of sound is shown in Figure 2. As can be seen, nearly all simulation results agree with the experiments within their statistical uncertainties. Figure 3 shows the performance for the thermal conductivity and shear viscosity for liquid states. Simulation results were obtained by equilibrium molecular dynamics simulations and the Green-Kubo formalism, cf. Guevara-Carrion *et al.*²⁹ The model slightly underpredicts the literature thermal conductivity data over the whole temperature range. For the shear viscosity, with the exception at 300 K, the simulation results agree with the literature data within their statistical uncertainties.

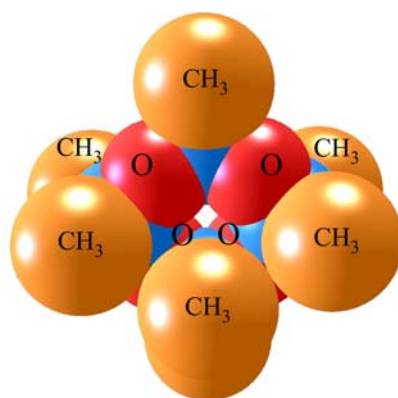


Figure 1. Present molecular interaction model for octamethylcyclotetrasiloxane. CH₃: methyl site, O: oxygen site, not labeled: silica site. Note that the sphere diameters correspond to the Lennard-Jones size parameters, which are depicted according to the molecular geometry scale.

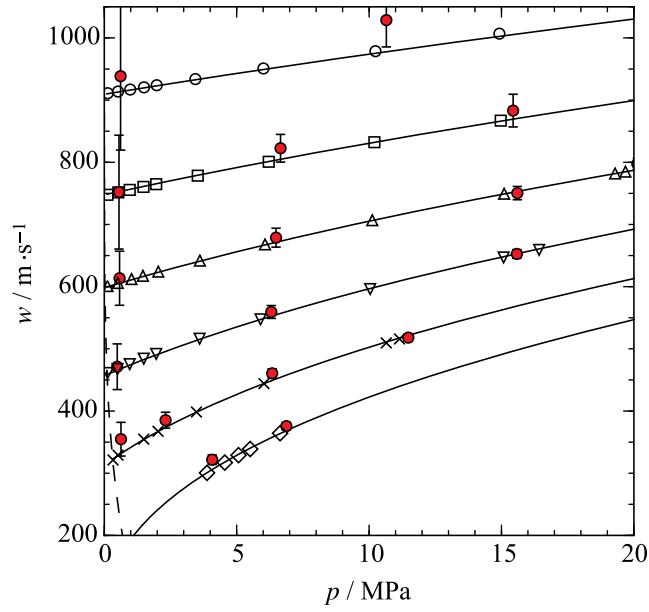


Figure 2. Speed of sound of octamethylcyclotetrasiloxane. Present experimental data: \circ 300 K, \square 350 K, Δ 400 K, ∇ 450 K, \times 500 K, \diamond 550 K; \circ (red) present simulation data; — present equation of state; - - vapor pressure curve.

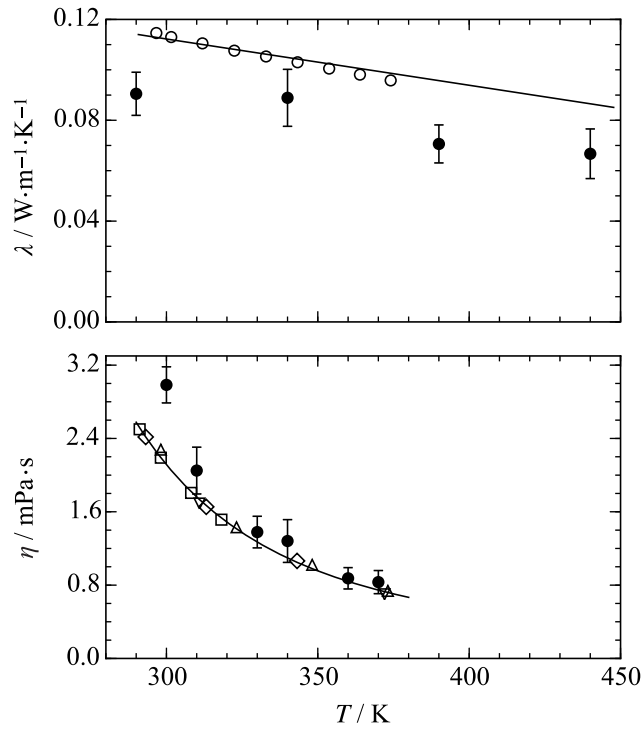


Figure 3. Thermal conductivity (top) and shear viscosity (bottom) of octamethylcyclotetrasiloxane at 0.1 MPa: \bullet present simulation data; experimental data by \circ Abbas *et al.*,³⁰ \square Marsh,³¹ \diamond Waterman *et al.*,³² Δ Reuther,³³ and ∇ Wilcock;³⁴ — correlation from the DIPPR database.³⁵

Table 1. Parameters of the present molecular interaction model for octamethylcyclotetrasiloxane. Lennard-Jones sites are denoted by the modeled atoms or atomic groups. Electrostatic sites are denoted by point charge magnitudes q . Coordinates (x, y, z) are given with respect to the center of mass in a principal axes system. k_B is the Boltzmann constant.

Interaction site	$x / \text{\AA}$	$y / \text{\AA}$	$z / \text{\AA}$	$\sigma / \text{\AA}$	$\varepsilon \cdot k_B^{-1} / \text{K}$	q / e
CH ₃	4.3198	-0.2718	1.3971	3.8181	122.4689	
CH ₃	3.9847	-1.7562	-1.3286	3.8181	122.4689	
Si	3.1365	-0.7701	0.0267	3.5167	15.2895	0.3036
O	1.9213	-1.6816	0.7475	3.1248	44.0134	-0.3036
CH ₃	1.6735	3.2187	-1.5120	3.8181	122.4689	
CH ₃	1.4331	2.2420	1.4613	3.8181	122.4689	
Si	1.3378	1.7784	-0.3619	3.5167	15.2895	0.3036
O	2.4782	0.5925	-0.7067	3.1248	44.0134	-0.3036
CH ₃	-2.2590	1.2815	1.3636	3.8181	122.4689	
CH ₃	-2.6052	-0.1997	-1.3611	3.8181	122.4689	
Si	-1.4157	0.2953	0.0056	3.5167	15.2895	0.3036
O	-0.2012	1.2041	-0.7199	3.1248	44.0134	-0.3036
CH ₃	0.2869	-2.6955	-1.4467	3.8181	122.4689	
CH ₃	0.0459	-3.7042	1.5158	3.8181	122.4689	
Si	0.3828	-2.2517	0.3814	3.5167	15.2895	0.3036
O	-0.7576	-1.0687	0.7370	3.1248	44.0134	-0.3036

3 EQUATION OF STATE

The equation of state presented here is expressed in terms of the molar Helmholtz energy a with the independent variables temperature T and density ρ . For a dimensionless description, the Helmholtz energy is reduced by the temperature and the universal gas constant R

$$\alpha(\tau, \delta) = \frac{a(T, \rho)}{RT}. \quad (3)$$

According to the theorem of corresponding states, the independent variables are reduced by the critical temperature T_c and critical density ρ_c . The reduced Helmholtz energy then reads

$$\alpha(\tau, \delta) = \alpha^o(\tau, \delta) + \alpha^r(\tau, \delta), \quad (4)$$

with $\tau = T_c/T$ and $\delta = \rho/\rho_c$. The ideal contribution (superscript “o”) is derived from an equation for the isobaric heat capacity

$$\frac{c_p^o}{R} = (c_0 + 1) + \sum_{i=1}^3 m_i \left(\frac{\theta_i}{T} \right)^2 \frac{\exp(\theta_i/T)}{(\exp(\theta_i/T) - 1)^2}. \quad (5)$$

Polynomial terms were avoided to ensure correct extrapolation behavior. Since the present fundamental equation of state is expressed in terms of the reduced Helmholtz energy, Eq. (5) has to be integrated twice with respect to τ

$$\alpha^o(\tau, \delta) = c^{II} + c^I \tau + c_0 \ln(\tau) + \sum_{i=1}^3 m_i \ln(1 - \exp(-\theta_i/T_c \tau)) + \ln(\delta). \quad (6)$$

The integration constants c^I and c^{II} can be chosen arbitrarily. For fluids that are liquids under standard conditions, the most common reference state is the normal boiling point. At $p = 1$ atm, the saturation temperature T_0 and the saturated liquid density ρ'_0 are determined. At this state point, the integration constants are chosen such that the enthalpy $h_0(T_0, \rho'_0) = 0 \text{ J}\cdot\text{mol}^{-1}$ and the entropy $s_0(T_0, \rho'_0) = 0 \text{ J}\cdot\text{mol}^{-1}\cdot\text{K}^{-1}$. The integration constants and the parameters for the Planck-Einstein terms are listed in Table 2.

Table 2. Parameters of the ideal part of the present equation of state (cf. Eq (6)).

i	1	2	3	c_0	c^I	c^{II}
m_i	0.292757	38.2456	58.975	3.0	-21.674365	71.163605
θ_i / K	40	200	1800			

The residual part (superscript “r”) comprises polynomial, exponential, and Gaussian bell-shaped terms

$$\begin{aligned}
\alpha^r(\tau, \delta) &= \alpha_{\text{Pol}}^r(\tau, \delta) + \alpha_{\text{Exp}}^r(\tau, \delta) + \alpha_{\text{GBS}}^r(\tau, \delta) \\
&= \sum_{i=1}^5 n_i \delta^{d_i} \tau^{t_i} + \sum_{i=6}^{10} n_i \delta^{d_i} \tau^{t_i} \exp(-\delta^{p_i}) \\
&\quad + \sum_{i=11}^{15} n_i \delta^{d_i} \tau^{t_i} \exp\left(-\eta_i (\delta - \varepsilon_i)^2 - \beta_i (\tau - \gamma_i)^2\right).
\end{aligned} \tag{7}$$

Polynomial and exponential terms are in principle sufficient for the description of the whole fluid surface. The Gaussian bell-shaped terms, introduced by Haar³⁶ and applied in a modified form to the fundamental equation of state for methane by Setzmann and Wagner,³⁷ allow for a more accurate representation of the critical region. Nowadays, these terms are used in all fluid regions, which leads to a reduction of the total number of terms. For a long time, equations with 20 to 50 terms were common practice,²⁴ whereas recent equations of state consist of 14 to 25 terms³⁸⁻⁴¹ due to this functional form. The present equation of state consists of 5 polynomial, 5 exponential, and 5 Gaussian bell-shaped terms. Its parameters are listed in Table 3.

Table 3. Parameters of the residual part of the present equation of state (cf. Eq. (7)).

<i>i</i>	<i>n_i</i>	<i>t_i</i>	<i>d_i</i>	<i>p_i</i>	<i>η_i</i>	<i>β_i</i>	<i>γ_i</i>	<i>ε_i</i>
1	5.273743·10 ⁻²	1.000	4	-				
2	4.176401·10 ⁺⁰	0.270	1	-				
3	-4.737070·10 ⁺⁰	0.510	1	-				
4	-1.289588·10 ⁺⁰	0.998	2	-				
5	5.272749·10 ⁻¹	0.560	3	-				
6	-2.558391·10 ⁺⁰	1.750	1	2				
7	-9.726737·10 ⁻¹	3.090	3	2				
8	7.208209·10 ⁻¹	0.790	2	1				
9	-4.789456·10 ⁻¹	2.710	2	2				
10	-5.563239·10 ⁻²	0.998	7	1				
11	3.766589·10 ⁺⁰	0.930	1	-	0.861	0.75	1.124	0.926
12	8.786997·10 ⁻²	3.170	1	-	1.114	0.55	1.388	1.300
13	-1.267646·10 ⁻¹	1.080	3	-	1.010	1.00	1.148	1.114
14	-1.004246·10 ⁺⁰	1.410	2	-	1.110	0.47	1.197	0.996
15	-1.641887·10 ⁺⁰	0.890	2	-	1.032	1.36	0.817	0.483

The equation presented here was constrained to the critical temperature $T_c = 586.5$ K of Young.⁴² The critical density $\rho_c = 1.043$ mol·dm⁻³ and the critical pressure $p_c = 1.347$ MPa were determined during the fit. The triple point temperature $T_{\text{tr}} = 290.25$ K of Mekhtiev and Karasharli⁴³ was applied as the lower temperature limit. The resulting triple point density is $\rho_{\text{tr}}^{\text{r}} = 3.24$ mol·dm⁻³. Additionally, the molecular weight $M = 296.61576$ g·mol⁻¹ was adopted.⁴⁴

The calculation of any thermodynamic state property via the derivatives of the reduced Helmholtz energy with respect to its independent variables can be taken from Span.²⁴

4 COMPARISON TO EXPERIMENTAL AND MOLECULAR SIMULATION DATA

In this section, the new equation of state is compared to experimental and molecular simulation data. An overview about homogeneous data is given in Figure 4. The grey area indicates the region covered by experimental measurements. The triangles depict the state points where molecular simulation data were generated in this work. In addition to these properties, vapor-liquid equilibrium and ideal-gas heat capacity data were available.

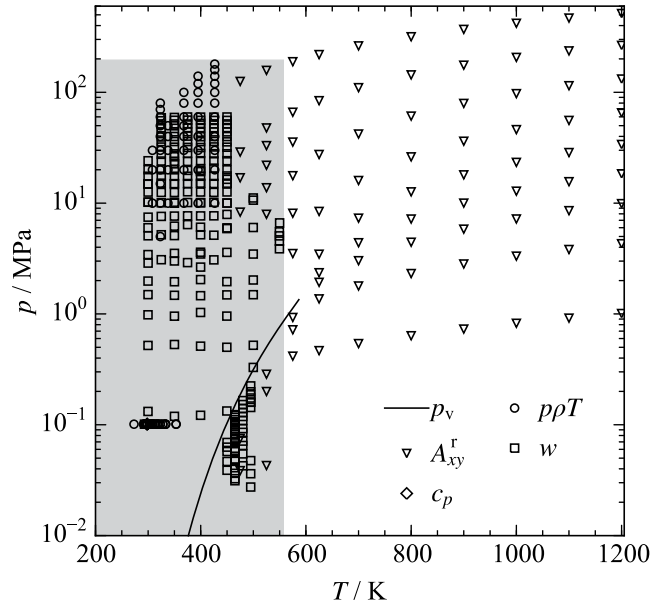


Figure 4. Available data for octamethylcyclotetrasiloxane in the homogeneous region. The grey area depicts the region where experimental data are available: $T_{\max} = 590$ K and $p_{\max} = 180$ MPa. The residual Helmholtz derivatives from molecular simulation extend this region up to $T_{\max} = 1200$ K and $p_{\max} = 520$ MPa.

In the next sections, the data analysis is based on relative deviations according to

$$\Delta X = 100 \frac{X_{\text{DATA}} - X_{\text{EOS}}}{X_{\text{DATA}}}. \quad (8)$$

Average absolute relative deviations (AAD) were calculated as follows

$$\text{AAD} = \frac{1}{N} \sum_{i=1}^N |\Delta X_i|. \quad (9)$$

For the statistical analysis, vapor pressure, saturated liquid density, and saturated vapor density data are separated into three temperature ranges: low temperature (LT: $T/T_c \leq 0.6$), medium temperature (MT: $0.6 \leq T/T_c \leq 0.98$), and high temperatures (HT: $T/T_c > 0.98$). All other properties are categorized as gas, liquid, critical region ($0.98 \leq T/T_c \leq 1.1$ and $0.7 \leq \rho/\rho_c \leq 1.4$), and supercritical region. The latter is further divided into low density (LD: $\rho/\rho_c \leq 0.6$), medium density (MD: $0.6 \leq \rho/\rho_c \leq 1.5$), and high density (HD: $\rho/\rho_c > 1.5$).

In the diagrams, the equation of Colonna *et al.*² and correlation equations of the DIPPR³⁵ and TDE⁴⁵ databases are plotted for comparison.

4.1 Ideal Gas State

In general, the ideal gas behavior of siloxanes has only been scarcely investigated. This challenge was discussed in detail by Thol *et al.*¹² and will only be summarized here briefly. When setting up the first set of Helmholtz equations, Colonna *et al.*² applied the Harrison-Seaton zeroth order contribution method.⁴⁶ This was the only method providing information about Si-C bonds. However, the DIPPR database³⁵ reports a possible uncertainty of up to 25 % for data from this method, which is not acceptable for accurate equations of state. Therefore, Nannan *et al.*⁴⁷ investigated the ideal gas behavior of several siloxanes more comprehensively. As a first approach, they measured speed of sound data for gaseous states, which they used to derive c_p° data. For small molecules, this is an accurate approach. However, with increasing complexity of the molecule, the uncertainty of this approach increases. A rough estimation can be made with the following relation²⁴

$$\left| \frac{\Delta c_p^\circ}{c_p^\circ} \right| = \left| 2 \left(\frac{c_p^\circ}{R} - 1 \right) \frac{\Delta w^\circ}{w^\circ} \right|. \quad (10)$$

Because of the large isobaric heat capacity of octamethylcyclotetrasiloxane, this results in an uncertainty of 3.9 % with respect to c_p° data although the speed of sound measurements are claimed to be accurate to within 0.02 %.⁴⁷ Since the measurements were carried out in a restricted temperature range (450 K to 495 K), these data are not sufficient to set up the ideal part for an equation of state covering the whole temperature range. Thus, Nannan *et al.*⁴⁷ determined c_p° data over a broad temperature range by means of *ab initio* calculations. They found similar results for two methods without giving any information on the accuracy of the data. Because the *ab initio* calculations were not done at the same temperatures as the measurements, the experiments cannot directly be used to assess the uncertainty of the calculations. The same calculations for hexamethyldisiloxane show a deviation from the corresponding equation¹² of approximately 3 %. Therefore, the c_p° data were only used as an approximate guide for the present fit. In Figure 5, the representation of the c_p° data of Nannan *et al.*⁴⁷ by the present equation of state is depicted. On the top, the reduced ideal gas heat capacity is illustrated as a function of temperature. For computational efficiency, Colonna *et al.*² applied a simple polynomial approach for their ideal gas equation of state, which does not extrapolate well. For $T \rightarrow 0$ K, only translational and rotational molecular degrees of freedom are excited,^{12,24} which leads to $c_p^\circ/R = 4$. The polynomial approach of Colonna *et al.*² results in an incorrect value of $c_p^\circ/R \approx -2$.

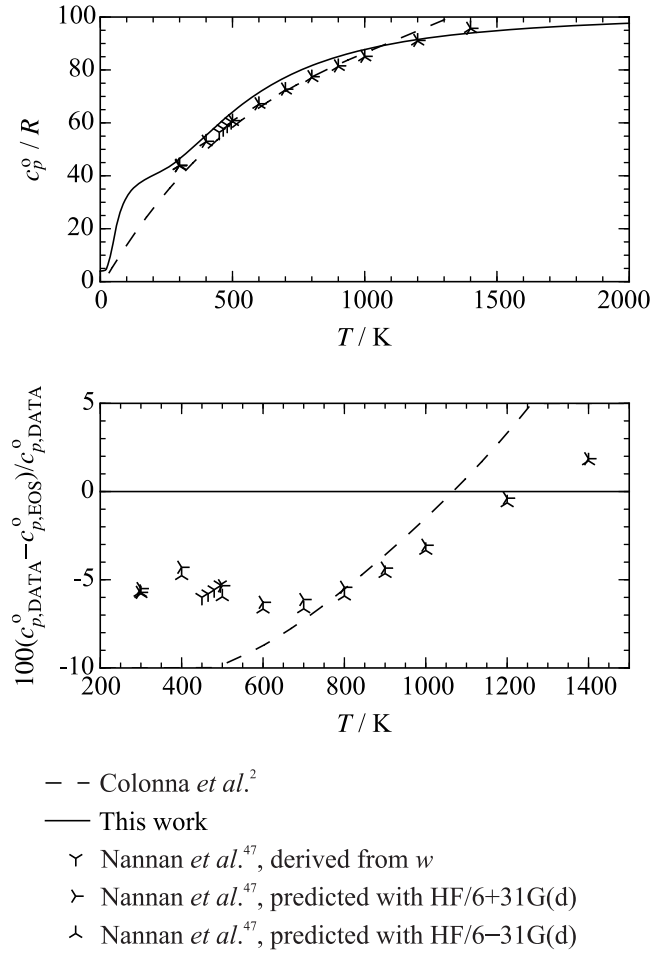


Figure 5. Representation of the isobaric heat capacity of the ideal octamethylcyclotetrasiloxane gas with the present equation of state.

For high temperatures, an asymptotic course with a limiting value based on the maximum number of molecular degrees of freedom has to be modeled. Due to the polynomial form, the ideal gas heat capacity of Colonna *et al.*² increases monotonously, whereas the present functional form reaches a limiting value. On the bottom of Figure 5, the three different methods of Nannan *et al.*⁴⁷ predicting c_p^0 data are compared to the present equation of state. For $T < 800$ K, the data systematically deviate by approximately 7 %. At higher temperatures, deviations decrease. The parameters of Eq. (5) were simultaneously adjusted to the c_p^0 data of Nannan *et al.*⁴⁷ and available data for the speed of sound and isobaric heat capacity (e.g., Refs.^{47,48}). During the fitting procedure, it turned out that it is not possible to represent the c_p^0 data in a more accurate way without compromising the other properties. Since the accuracy of the c_p^0 data is questionable, the speed of sound and isobaric heat capacity data were preferentially fitted and the comparably high deviations of the c_p^0 data have to be accepted here.

4.2 Vapor-Liquid Equilibrium

Available experimental vapor pressure data are summarized in Figure 6 and Table 4. Many authors report vapor pressure data in their publications to point out the purity of their sample. More comprehensive investigations were made by 8 research groups, which are discussed in more detail here. As an indication for the quality of the data, the measurements of hexamethyldisiloxane, which were analyzed comprehensively by Thol *et al.*,¹² were considered where groups published data for both fluids. The lower temperature region ($T < 460$ K) was investigated by several different authors, whereas the higher temperature region was studied only by Young.⁴² In the lower temperature region the present equation of state was fitted to Flaningam's⁴⁹ vapor pressure data (AAD = 0.76 %). He reported these measurements in the same publication as the results for hexamethyldisiloxane. Deviations of 0.5 % with respect to the equation for hexamethyldisiloxane were assessed to be reasonable.¹² The experimental uncertainty of the octamethylcyclotetrasiloxane data is assumed to be higher than in the case of hexamethyldisiloxane due to an inferior sample purity (octamethylcyclotetrasiloxane: 99.49 %, hexamethyldisiloxane 99.9 %) and the deviations of less than 1.1 % with respect to the present equation of state seem to be realistic. In this way, the data of Marsh^{50,51} and Tomlins and Marsh⁵² scatter around the equation within 1.5 % for $T < 360$ K. Since the vapor pressure of Tomlins and Marsh⁵² was measured more recently than the data of Marsh,^{50,51} this point was taken as a reference and was reproduced within 0.063 % by the present equation of state. Fitting the data of Flaningam⁴⁹ in a more accurate way would cause higher deviations in the low temperature regime. In the temperature region where Flaningam's⁴⁹ data are located, recent measurements of Abbas *et al.*⁴⁸ (AAD = 4.79 %) are available. In analogy to the results for hexamethyldisiloxane, these data significantly differ from the present equation and other literature data. Between 370 K and 451 K, a systematic offset of approximately -2.7 % can be observed. Deviations increase for lower temperatures, which is most probably caused by an inappropriate handling of the apparatus, cf. Thol *et al.*¹² The data of Stull⁵³ (AAD = 8.60 %) are part of a comprehensive literature study summarizing vapor pressure data for more than 1200 organic substances. In this publication,⁵³ Hunter *et al.*,⁵⁴ Patnode and Wilcock,⁵⁵ and Wilcock³⁴ are cited to be the primary sources for octamethylcyclotetrasiloxane. In the original publications,^{34,54,55} all of them investigated siloxane polymers and they only report the normal boiling point of the participating monomers. Since Stull's⁵³ data exhibit unreasonably high deviations of up to 20 %, they were not considered any further. Korchemskaya *et al.*⁵⁶ (AAD = 2.44 %) primarily investigated binary mixtures containing siloxanes and only report uncertainties in terms of composition. No information is given for the uncertainty of the pure fluid data. Except for two state points at $T \geq 444$ K, the measured vapor pressures are systematically lower than values calculated from the present equation of state. However, they are still reproduced within 1.1 %, which is the same accuracy as for the data of Flaningam.⁴⁹

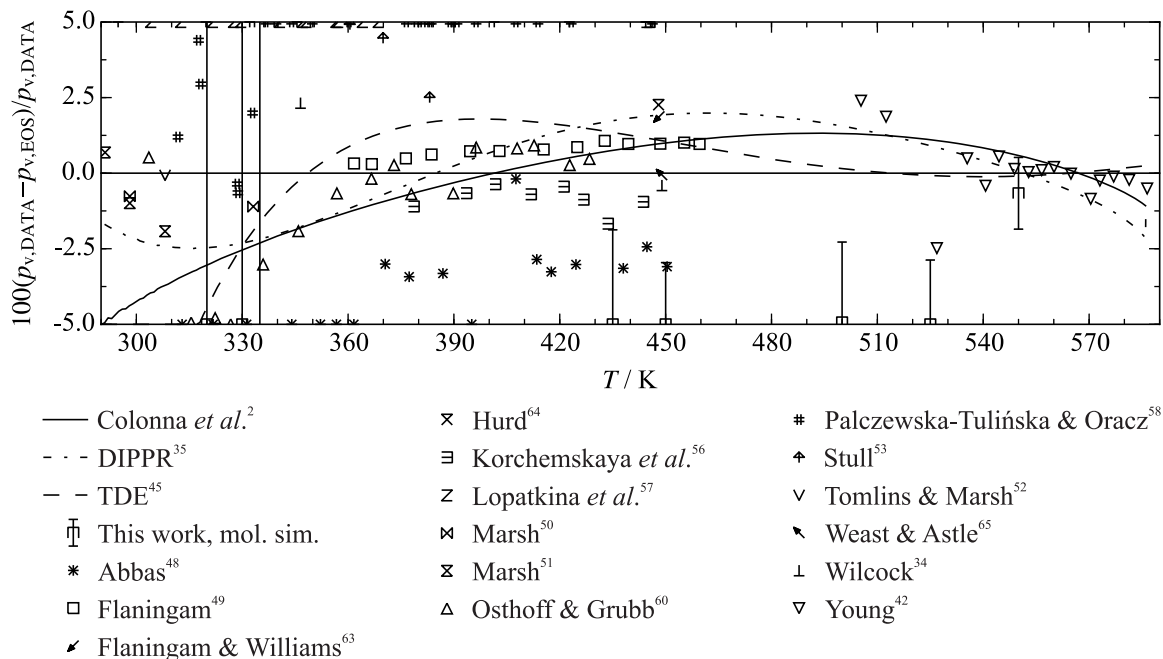


Figure 6. Relative deviations of the vapor pressure data from the present equation of state.

Lopatkina *et al.*⁵⁷ (AAD = 20.4 %) measured the vapor pressure between 304 K to 369 K by means of a static method with a quartz Bourdon gauge as a reference. The temperature was controlled with copper-constantan thermocouples. No information on the experimental uncertainties is given. Deviations with respect to the present equation of state increase from 5 % to 38 % with decreasing temperature. The measurements of Marsh,^{50,51} which are located in the same temperature range, indicate that the data of Lopatkina *et al.*⁵⁷ are most likely not correct. Therefore, these data were not considered during the development of the present equation of state. Recent measurements of Palczewska-Tulińska and Oracz⁵⁸ were carried out with a comparative ebulliometer applying n-dodecane as the reference substance. The specified temperature uncertainty $\Delta T = 0.005$ K and pressure uncertainty $\Delta p = 6.7$ Pa yield a combined expanded uncertainty of 0.03 % to 3.8 % ($k = 2$). Measurements of Palczewska-Tulińska *et al.*⁵⁹ on cyclohexane were made with the same technique and are reproduced by the equation of Zhou *et al.*⁴¹ with an AAD = 0.13 %. Nonetheless, the measurements of octamethylcyclotetrasiloxane exhibit deviations of up to 8.5 % with respect to the present equation of state and other measurements in this region. Data at lower temperatures deviate significantly less than at high temperatures. These findings agree with their own correlation results presented in Ref.⁵⁸ A similar behavior is present for hexamethylcyclotrisiloxane and even worse deviations were observed for decamethylcyclopentasiloxane. Therefore, the data were not considered during the development of the present equation of state. Finally, measurements of Osthoff and Grubb⁶⁰ (AAD = 1.69 %) are available in the same temperature range as the data sets discussed above. The sample purity was estimated to be 99.82 % based on a melting point measurement. For the vapor pressure measurements, a modified isoteniscope of Smith and Menzies,⁶¹ which is categorized as a static method, was used. No

information is given about the experimental uncertainties. For $T \geq 350$ K, deviations with respect to the present equation of state amount to 1 %, which is in accordance with the data of Flaningam⁴⁹ and Korchemskaya *et al.*⁵⁶ For lower temperatures ($T < 350$ K), the percentage deviations increase. This is most likely related to the pressure measurement, which was carried out with a mercury manometer. Since the vapor pressure of octamethylcyclotetrasiloxane is low, only a small column of mercury was observed (1.49 mmHg at the lowest temperature). The percentage deviations from the equation yield systematic absolute deviations of approximately -0.3 mmHg. These differences can easily occur with a visual detection of the meniscus. Furthermore, the vapor pressure at the lowest temperature agrees well with the data point of Tomlins and Marsh.⁵² Thus, the increasing deviations of the data with respect to the present equation are assumed to be a problem in the data. In their publication, Osthoff and Grubb⁶⁰ introduced a correction for all vapor pressure data at $T \geq 353$ K by adding the vapor pressure of mercury. No further explanation for why they did not do the same correction for the low temperature data was provided. The only experimental data set available for $T > 460$ K was published by Young⁴² (AAD = 0.67 %). A modified glass apparatus of Ambrose and Townsend⁶² was used and the specified uncertainty amounts to 0.5 % to 2 %. Except for two data points with deviations of 2.5 %, all of their data scatter around the present equation of state within the given experimental uncertainty. Based on these results, the expected uncertainty of vapor pressure data calculated with the present equation of state is 1.5 % for $T \leq 460$ K and 2 % for higher temperatures.

Table 4. Average absolute relative deviations of experimental vapor pressure data and saturated liquid and vapor densities from the present equation of state. All temperatures were adapted to the ITS-90 scale. Data sets, which were applied to the fit, are marked with an asterisk.

Authors	No. of data	Temperature range / K	Average absolute relative deviation (AAD) / %			Overall
			LT ^a	MT ^a	HT ^a	
Vapor pressure p_v						
Abbas <i>et al.</i> ⁴⁸	18	312 - 451	7.56	4.00	-	4.79
Flaningam ^{49*}	13	361 - 460	-	0.76	-	0.76
Flaningam & Williams ⁶³	1	448.15	-	1.87	-	1.87
Hurd ⁶⁴	1	447.99	-	2.26	-	2.26
Korchemskaya <i>et al.</i> ⁵⁶	10	378 - 446	-	2.44	-	2.44
Lopatkina <i>et al.</i> ⁵⁷	12	304 - 369	26.5	8.14	-	20.4
Marsh ⁵⁰	2	298 - 334	0.94	-	-	0.94
Marsh ⁵¹	3	291 - 309	1.20	-	-	1.20
Osthoff & Grubb ⁶⁰	16	303 - 429	3.53	0.58	-	1.69
Palczewska-Tulińska & Oracz ⁵⁸	24	311 - 447	3.40	8.04	-	6.10
Stull ⁵³	10	294 - 445	12.5	5.97	-	8.60
Tomlins & Marsh ⁵²	1	308.14	0.063	-	-	0.063
Weast & Astle ⁶⁵	1	448.91	-	0.054	-	0.054

Authors	No. of data	Temperature range / K	Average absolute relative deviation (AAD) / %			Overall
			LT ^a	MT ^a	HT ^a	
Vapor pressure p_v						
Wilcock ³⁴	2	346 - 449	2.32	0.40	-	1.36
Young ^{42*}	16	505 - 587	-	0.75	0.28	0.67
Saturated liquid density ρ'						
Golik & Cholpan ⁶⁶	1	303.13	0.29	-	-	0.29
Hurd ⁶⁴	5	273 - 354	4.64	0.017	-	3.72
Korchemskaya <i>et al.</i> ⁵⁶	1	293.14	0.035	-	-	0.035
Levien ⁶⁷	1	298.14	0.024	-	-	0.024
Marsh ⁵¹	3	291 - 309	0.044	-	-	0.044
McLure & Barbarin-Castillo ^{68*}	14	292 - 409	0.006	0.028	-	0.015
Palczewska-Tulińska & Oracz ⁵⁸	22	292 - 434	0.13	0.17	-	0.15
Patnode & Wilcock ⁵⁵	1	293.14	0.066	-	-	0.066
Shinoda & Hildebrand ⁶⁹	1	298.14	0.005	-	-	0.005
Tanaka ⁷⁰	1	293.14	0.066	-	-	0.066
Tomlins & Marsh ⁵²	1	308.14	0.043	-	-	0.043
Waterman <i>et al.</i> ³²	1	293.14	0.030	-	-	0.030
Young ^{42*}	7	503 - 577	-	0.24	0.44	0.26
Saturated vapor density ρ''						
Korchemskaya <i>et al.</i> ⁵⁶	9	378 - 446	-	6.19	-	6.19
Young ⁴²	8	536 - 580	-	10.5	18.5	11.5

^a LT: $T/T_c \leq 0.6$; MT: $0.6 \leq T/T_c \leq 0.98$; HT: $T/T_c > 0.98$

The representation of the saturated liquid and vapor densities is depicted in Figure 7 and the average absolute relative deviations are listed in Table 4. Similar to the vapor pressure, the lower temperature region was measured by different authors, whereas the high temperature region was only investigated by Young.⁴² The most comprehensive data sets for $T < 440$ K were published by McLure and Barbarin-Castillo⁶⁸ (AAD = 0.015 %) and Palczewska-Tulińska and Oracz⁵⁸ (AAD = 0.15 %). Palczewska-Tulińska and Oracz⁵⁸ used an Anton Paar densimeter and the specified uncertainties yield a combined expanded uncertainty of approximately 0.006 % in density. Most probably, the stated uncertainty of the density measurement $\Delta\rho = 0.01 \text{ kg}\cdot\text{m}^{-3}$ is too optimistic so that the real uncertainty is assumed to be higher. In comparison to the present equation of state and other literature data, the data of Palczewska-Tulińska and Oracz⁵⁸ differ by up to 0.4 %. The deviations exhibit a parabolic shape, which is the same behavior as for their measurements of decamethylcyclopentasiloxane.⁵⁸ This leads to the assumption that either the apparatus or the measurement procedure was incorrect. Thus, the remaining data set of McLure and Barbarin-Castillo⁶⁸ was used to develop the present equation of state. The sample was purified up to 99.5 % and the measurements were carried out with a magnetically levitated Archimedian

sinker.⁶⁸ The specified uncertainties result in a combined expanded uncertainty ($k = 2$) of 0.014 %. For $T < 360$ K, the present equation of state reproduces the data within their experimental uncertainty. With increasing temperature, the deviations increase up to 0.4 %. This is caused by the high temperature data of Young⁴² (AAD = 0.26 %), which scatter around the present equation of state within 0.45 %. For each measurement, Young⁴² filled a glass tube with liquid octamethylcyclotetrasiloxane, evacuated the tube while freezing the sample, and sealed the tube after degassing. Subsequently, each tube was heated slowly and the temperature was detected at which the tube was completely filled with liquid. The mass of the sample was determined by weighing the sealed tube including the sample, and subsequent weighing the opened tube that was purged of the sample. The volume was determined by measuring the weight of the full and cut tube in distilled water. These three steps involve several different sources of uncertainties, which are not discussed in the paper. However, Young⁴² states an uncertainty of 0.1 % to 0.3 %. Since it is not completely clear how the experimental uncertainty was determined, deviations of 0.45 % with respect to the present equation of state seem to be acceptable.

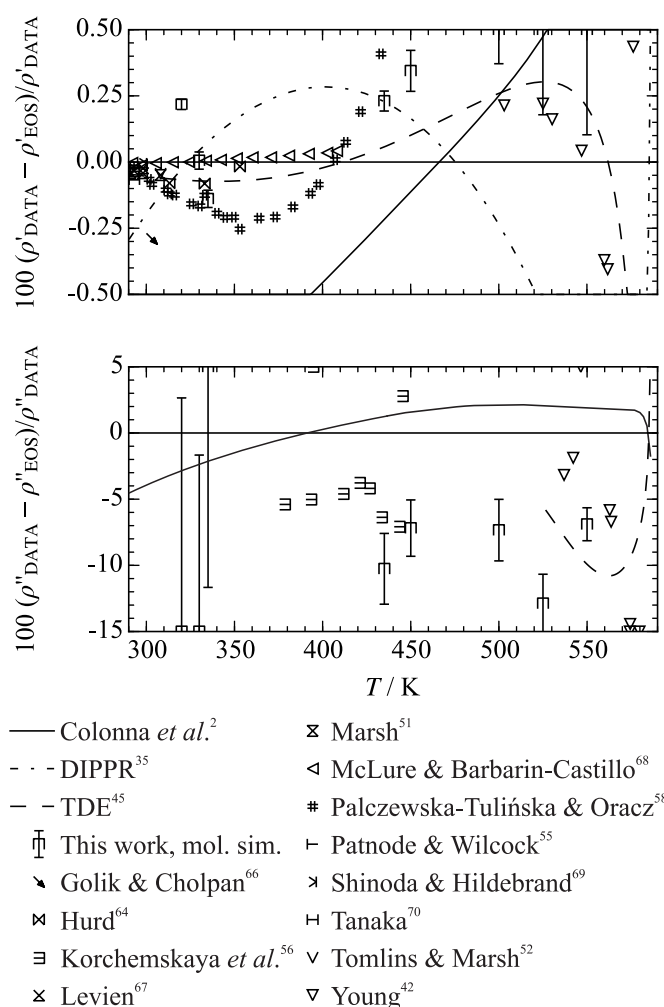


Figure 7. Relative deviations of the saturated density data from the present equation of state. Top: saturated liquid density, bottom: saturated vapor density.

Finally, the data sets comprising only few state points were used to verify the representation of the saturated liquid density. The data of Korchemskaya *et al.*,⁵⁶ Levien,⁶⁷ Marsh,⁵¹ Patnode and Wilcock,⁵⁵ Tanaka,⁷⁰ Tomlins and Marsh,⁵² and Waterman *et al.*³² are reproduced with an AAD < 0.07 %. Therefore, the uncertainty of saturated liquid density data calculated with the present equation of state is assessed to be 0.1 % for $T < 360$ K and 0.5 % for higher temperatures.

The saturated vapor density was investigated by Korchemskaya *et al.*⁵⁶ (AAD = 6.19 %) and Young⁴² (AAD = 11.5 %). Korchemskaya *et al.*⁵⁶ focused on mixture measurements and did not provide information on the experimental uncertainties. Young⁴² applied the same measuring procedure as for the saturated liquid density. The disappearance of the corresponding phases was detected visually and thus lead to higher uncertainties. For the liquid phase, a remaining gas bubble does not falsify the result too much, whereas a remaining liquid droplet in the gaseous phase has a large impact. Therefore, the deviations presented in Figure 7 are not surprising. For a reliable uncertainty statement, a more appropriate measuring technique has to be used to carry out new measurements.

4.3 Homogeneous Region

Comparisons to homogeneous density data are shown in Figure 8 and summarized in Table 5. At the bottom of Figure 8, relative deviations of experimental data from the present equation of state at atmospheric pressure are illustrated. The temperature range is restricted to 290 K to 355 K. Except for the data by Schuh and Fischer,⁷¹ all data deviate by less than 0.1 % from the present equation. The measurements of Marsh⁵⁰ (AAD = 0.058 %) and Herring and Winnick⁷² (AAD = 0.056 %) agree perfectly with each other and are reproduced within 0.06 %. An even better representation of the data was not possible without compromising the saturated liquid density.

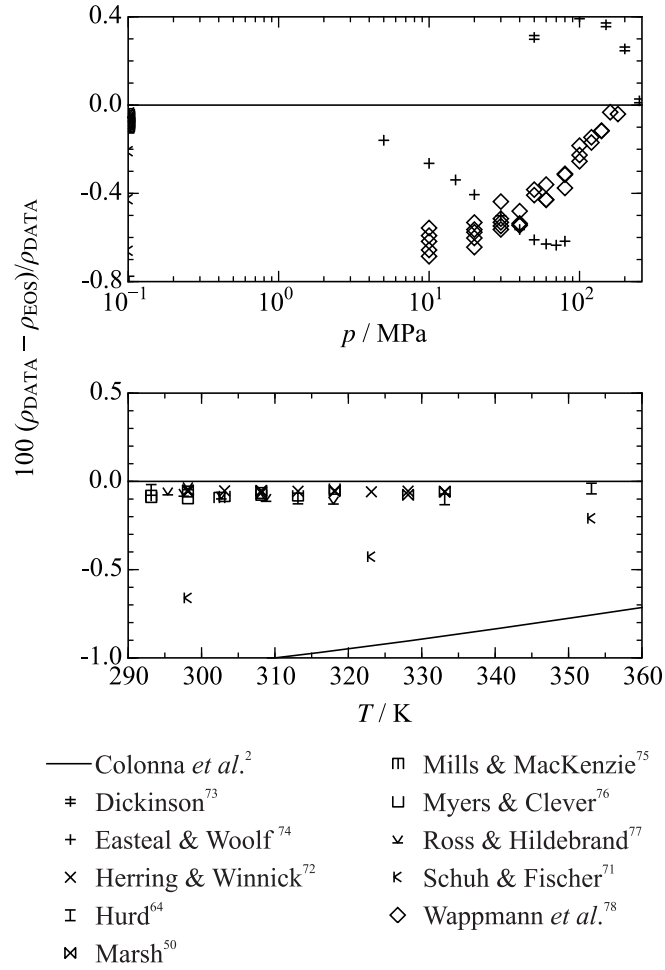


Figure 8. Representation of the homogeneous density of octamethylcyclotetrasiloxane. Top: Relative deviations of all available experimental homogeneous density data from the present equation of state. Bottom: Relative deviations of the homogeneous density data from the present equation of state at atmospheric pressure.

Table 5. Average absolute relative deviations of the experimental data in the homogeneous state from the present equation of state. All temperatures were adapted to the ITS-90 scale. Data sets, which were applied to the fit, are marked with an asterisk. For the ppT data in the critical region, pressure deviations are considered instead of density deviations. Critical region: $0.98 \leq T/T_c \leq 1.1$ and $0.7 \leq \rho/\rho_c \leq 1.4$; Supercritical region: LD: $\rho/\rho_c \leq 0.6$; MD: $0.6 < \rho/\rho_c \leq 1.5$; HD: $\rho/\rho_c > 1.5$.

Authors	No. of data	Temperature and pressure range		Average absolute relative deviation (AAD) / %						
		T / K	p / MPa	Gas	Liq.	Crit. reg.	LD	MD	HD	overall
ppT data										
Dickinson ^{73a}	5	323.19	50.0 - 251	-	0.27	-	-	-	-	0.27
Eastal & Woolf ⁷⁴	10	323.19	5.0 - 81	-	0.47	-	-	-	-	0.47
Herring & Winnick ⁷²	8	298 - 334	0.101325	-	0.056	-	-	-	-	0.056
Hurd ⁶⁴	5	273 - 354	0.101325	-	3.74	-	-	-	-	3.74
Marsh ⁵⁰	5	298 - 334	0.101325	-	0.058	-	-	-	-	0.058
Mills & MacKenzie ⁷⁵	2	293 - 303	0.101325	-	0.087	-	-	-	-	0.087

Authors	No. of data	Temperature and pressure range		Average absolute relative deviation (AAD) / %						
		T / K	p / MPa	Gas	Liq.	Crit. reg.	LD	MD	HD	overall
Myers & Clever ⁷⁶	6	293 - 319	0.101325	-	0.078	-	-	-	-	0.078
Ross & Hildebrand ⁷⁷	6	295 - 318	0.101325	-	0.071	-	-	-	-	0.071
Wappmann <i>et al.</i> ^{78*}	36	308 - 427	10.0 - 181	-	0.42	-	-	-	-	0.42
Schuh & Fischer ⁷¹	3	298 - 354	0.101325	-	0.43	-	-	-	-	0.43
Speed of sound w										
This work*	54	299 - 550	0.1 - 27	-	0.12	-	-	-	0.15	0.14
Golik & Cholpan ⁷⁹	1	303.13	0.101325	-	0.15	-	-	-	-	0.15
Nannan <i>et al.</i> ^{47*}	53	450 - 496	0.0 - 1.0	0.17	-	-	-	-	-	0.17
Niepmann & Schmidt ⁸⁰	117	299 - 450	2.6 - 61	-	-	-	-	-	0.47	0.47
Waterman <i>et al.</i> ³²	1	293.14	0.101325	-	0.026	-	-	-	-	0.026
Isobaric heat capacity c_p										
Abbas <i>et al.</i> ^{48*}	28	298 - 434	0.101325	-	0.18	-	-	-	-	0.18
Marsh & Tomlins ⁸¹	1	298.14	0.101325	-	1.81	-	-	-	-	1.81
Mekhtiev & Karasharli ⁴³	1	298.14	0.101325	-	2.73	-	-	-	-	2.73
Palczewska-Tulińska & Orcz ⁵⁸	24	293 - 426	p_v	-	2.05	-	-	-	-	2.05

^a calculated

Since the measured saturated liquid density data cover the entire vapor-liquid equilibrium temperature range and the homogeneous density measurements are restricted to a range of 65 K, the saturated liquid density was primarily correlated. However, reproducing the homogeneous density data at atmospheric pressure in a more accurate way is most probably not required, because deviations can be explained by the claimed experimental uncertainty of the data. The correlation of the high pressure data was more challenging, because contradictory trends were observed (cf. Figure 8, top). Wappman *et al.*⁷⁸ utilized a sample with a purity of 99 % for their measurements. The employed piston cylinder densimeter was described by Wappmann *et al.*⁸² in detail. The accuracy of the measurements was assessed with test measurements of methanol, which reproduced Goodwin's⁸³ data within 0.2 %. Without any further explanation, Wappmann *et al.*⁷⁸ state an experimental uncertainty of 0.4 % for octamethylcyclotetrasiloxane. The second data set of Easteal and Woolf⁷⁴ shows an opposite trend with respect to the present equation of state. They investigated only one isotherm (323.15 K), which was not measured by Wappmann *et al.*⁷⁸ Therefore, it is not possible to compare these results directly with each other. Easteal and Woolf⁷⁴ measured their density data with an even lower sample purity (98 %) than Wappmann *et al.*⁷⁸ in a bellows volumeter.⁸⁴ The specified uncertainties yield a combined expanded uncertainty of 0.06 %, a value that is highly unrealistic considering the sample purity. It was not possible to represent

any of the data within the claimed accuracy. Thus, test correlations were established to find out what is causing these problems. Fitting both data sets at the same time is not possible due to their contrary courses. Therefore, only one data set was correlated at a time and it was still not possible to reach a satisfactory result. Hence, the interaction of different properties was investigated. Next to homogeneous density data, speed of sound measurements of this work and isobaric heat capacity data of Abbas *et al.*⁴⁸ recently became available. Both data sets were considered in the fitting procedure. Since Abbas *et al.*⁴⁸ heat capacity measurements were reasonable for hexamethyldisiloxane,¹² it is unlikely that these data cause problems. As expected, no observable improvement of the density data could be reached when deleting these data from the fit. Therefore, the present speed of sound measurements were tested. After deleting these data from the fit, the requested result was achieved. The homogeneous density data of Wappmann *et al.*⁷⁸ could be fitted significantly better than before. Hence, both data sets are not consistent with each other. The definition of the speed of sound explains this effect

$$w^2 = \frac{c_p}{c_v} \left(\frac{\partial p}{\partial \rho} \right)_T. \quad (11)$$

One of the two data sets comprises a wrong course of the compressibility so that the other data set cannot be correlated within the required accuracy. Since there is no independent data set for the homogeneous density available, which could support the data of Wappmann *et al.*,⁷⁸ the present speed of sound measurements were chosen to be primarily fitted.

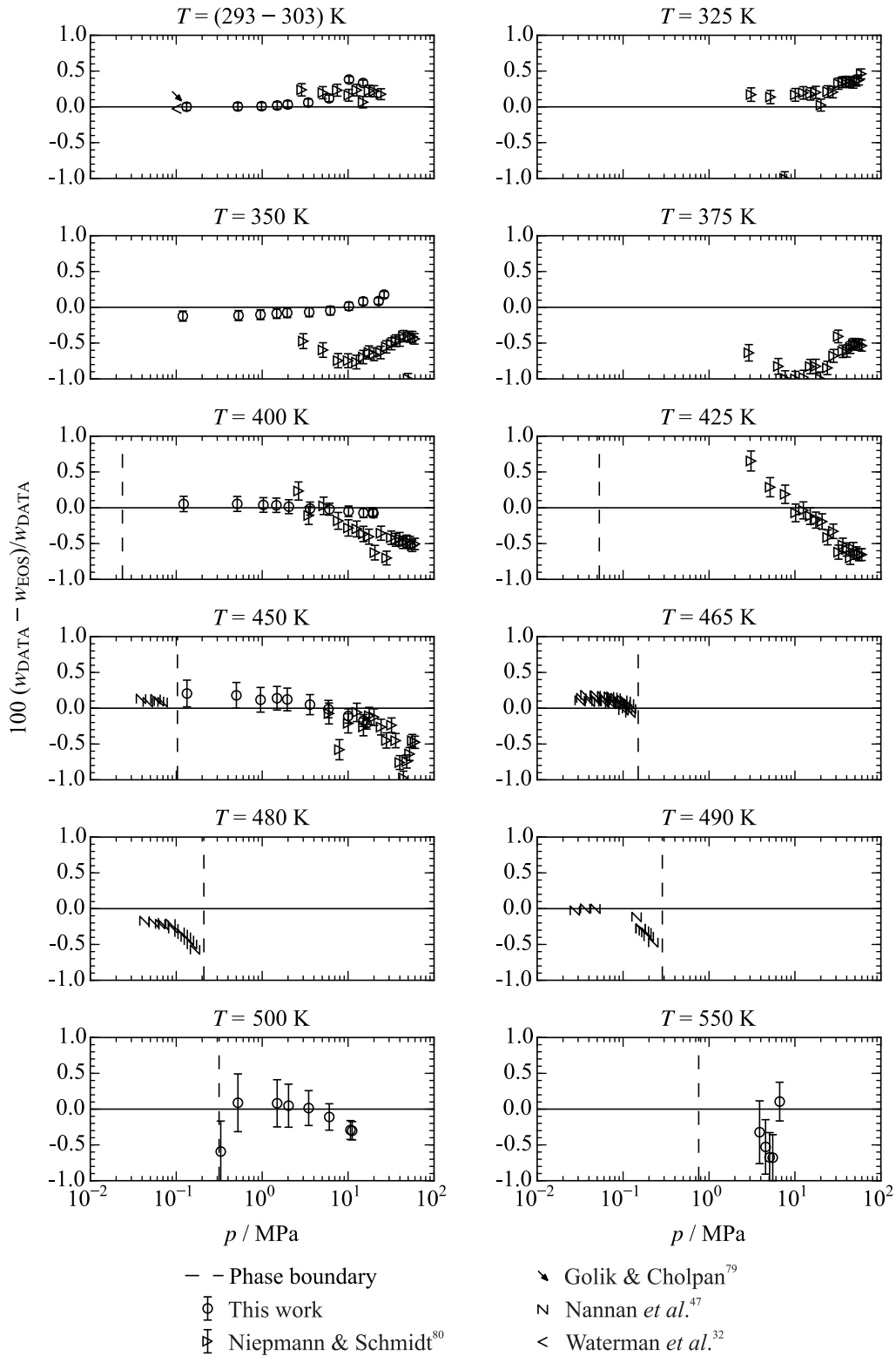


Figure 9. Relative deviations of experimental speed of sound data from the present equation of state.

For the present speed of sound measurements, the same apparatus was utilized as for hexamethyldisiloxane,¹² ammonia,¹⁴ oxygen,⁸⁵ and hydrogen chloride. In general, the data could be reproduced within 0.5 % by the corresponding equations of state so that this accuracy was also aimed at in the case of octamethylcyclotetrasiloxane. Figure 9 shows that the speed of sound data are represented by the present equation of state within the specified

experimental uncertainties. Additional speed of sound data located in the liquid phase were published by Niepmann *et al.*⁸⁰ They employed an accurate pulse-echo method, which was also used in the present work. The reported uncertainty of $0.8 \text{ m}\cdot\text{s}^{-1}$ corresponds to a relative uncertainty of 0.1 %. However, with the same apparatus they measured speed of sound data for benzene, which scatter around the corresponding equation of state of Thol *et al.*⁴⁰ within 0.4 %. Therefore, the relative deviations of approximately 0.5 %, except for the isotherms 350 K and 375 K, are plausible. Accepting these deviations in the liquid speed of sound data, a relative deviation of the density data of Wappmann *et al.*⁷⁸ from the present equation of 0.65 % could be achieved. The data of Eastal and Woolf⁷⁴ deviate in the same range. Finally, the speed of sound data in the gaseous state of Nannan *et al.*,⁴⁷ which were already discussed in the ideal gas section, are shown in Figure 9. Relative deviations are 0.16 % for $T \leq 465 \text{ K}$ and increase up to 0.45 % for higher temperatures. The large deviations occur close to the saturated vapor phase, whereas deviations decrease in the limit of low pressures. This trend proves a reasonable ideal gas contribution α^0 of the present equation of state.

Summarizing the discussion above, the homogeneous density can be calculated from the present equation of state within 0.1 % at atmospheric pressure and 0.7 % for higher pressures. Vapor phase measurements are not available so that no statement on the accuracy of the present equation of state can be made. Speed of sound data in the liquid and vapor state can be calculated from the present equation with an expected uncertainty of 0.5 %

In Figure 10, comparisons of available experimental isobaric heat capacity data with the present equation of state are depicted. The two main data sets were published by Abbas *et al.*⁴⁸ (AAD = 0.18 %) and Palczewska-Tulińska and Oracz⁵⁸ (AAD = 2.05 %) and exhibit a contrary course. In accordance to the previous discussion on vapor pressure and saturated liquid density, significant deviations of the heat capacity measurements in the saturated liquid state of all substances investigated in the publication of Palczewska-Tulińska and Oracz⁵⁸ with respect to other literature data can be observed. Therefore, these data were not considered during the development of the present equation of state. The isobaric heat capacity data for hexamethyldisiloxane measured at atmospheric pressure by Abbas *et al.*⁴⁸ showed good agreement with the corresponding equation and other literature data, cf. Thol *et al.*¹² Therefore, the data for octamethylcyclotetrasiloxane were assumed to be reliable and were used in the fit. A relative deviation of 0.3 % could be achieved, which is clearly within the experimental uncertainty of 1 % as stated by the authors. Thus, the expected uncertainty of heat capacity data in the saturated liquid state calculated with the present equation of state is 1 % according to the experimental uncertainty of the data of Abbas *et al.*⁴⁸

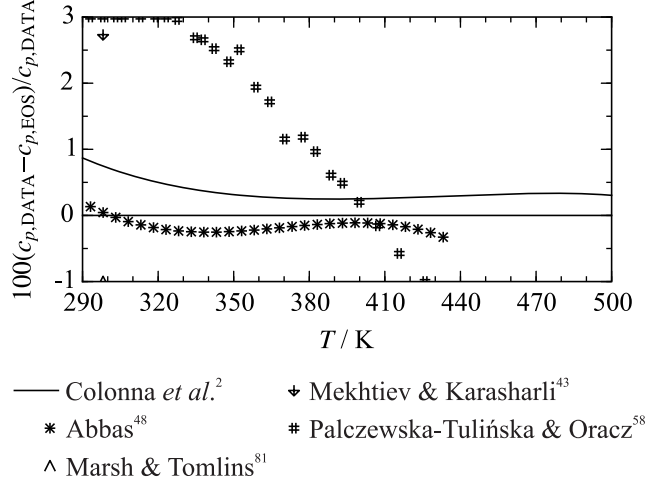


Figure 10. Relative deviations of experimental isobaric heat capacity data from the present equation of state.

4.4 Representation of Molecular Simulation Data

After fitting the present equation of state exclusively to experimental measurements, molecular simulation data up to 1200 K and 520 MPa were added to the data set used in the fit in order to extend the range of validity. Since the molecular structure of octamethylcyclotetrasiloxane is not stable at such high temperatures and pressures, this extension of the validity range has to be perceived as an extrapolation beyond the stable region. The simulated vapor pressure data differ by up to 10 % for $T \geq 435$ K. Lower temperatures are reproduced even worse. However, the simulated saturated liquid density data differ from the present equation of state within the stated accuracy of 1 %, except for the highest temperature $T = 550$ K. The accuracy of the molecular model in the homogeneous region was assessed by simulations of density and speed of sound at selected state points (cf. Figure 11). The homogeneous density is represented within 0.7 %, which is the expected uncertainty of the present equation of state. The simulated $p\rho T$ data support the course of the density calculated from the equation of state, which resulted primarily from a fit to saturated liquid density and speed of sound data, rather than from a fit to the available $p\rho T$ data. The gaseous speed of sound data differ by 1.3 % from the present equation of state, whereas the liquid state points deviate by up to 15 %. The differences become evident from the following equation

$$w^2/(RT) = 1 + 2A_{01}^r + A_{02}^r - \frac{(1 + A_{01}^r - A_{11}^r)^2}{A_{20}^o + A_{20}^r}. \quad (12)$$

The speed of sound is composed of several residual Helmholtz derivatives and the ideal gas heat capacity, which is considered by A_{20}^o . Because only the residual parts are simulated, the ideal gas part is taken from the present equation of state. In the gaseous phase, the ideal gas contribution is the dominating part, which compensates uncertainties of the simulated residual

Helmholtz derivatives. The liquid state is prevailed by the residual contribution so that the impact of the ideal gas contribution is smaller, which leads to higher deviations.

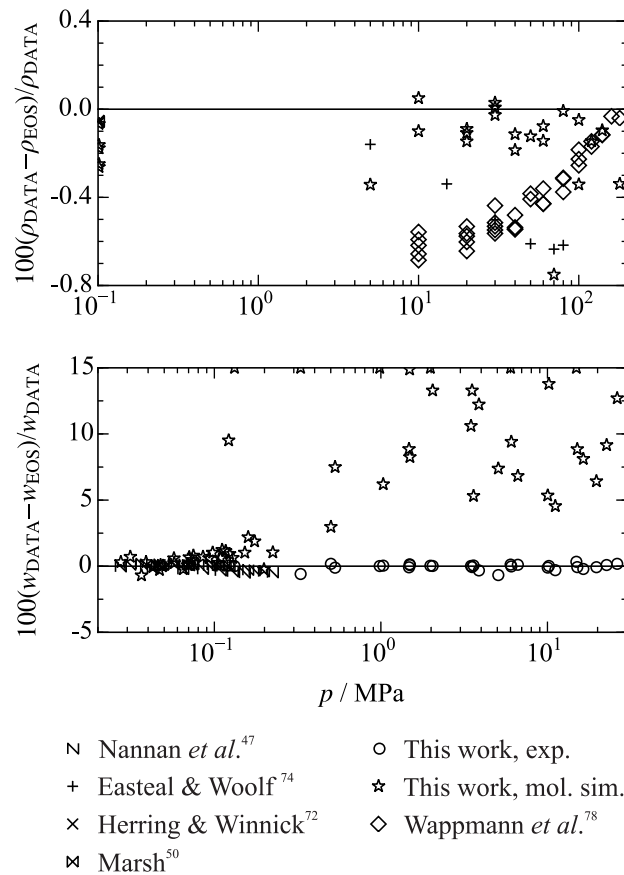


Figure 11. Relative deviations of selected density (top) and speed of sound (bottom) data from the present equation of state. At the same p - T state points, molecular simulation data are presented to verify the accuracy of the present molecular model.

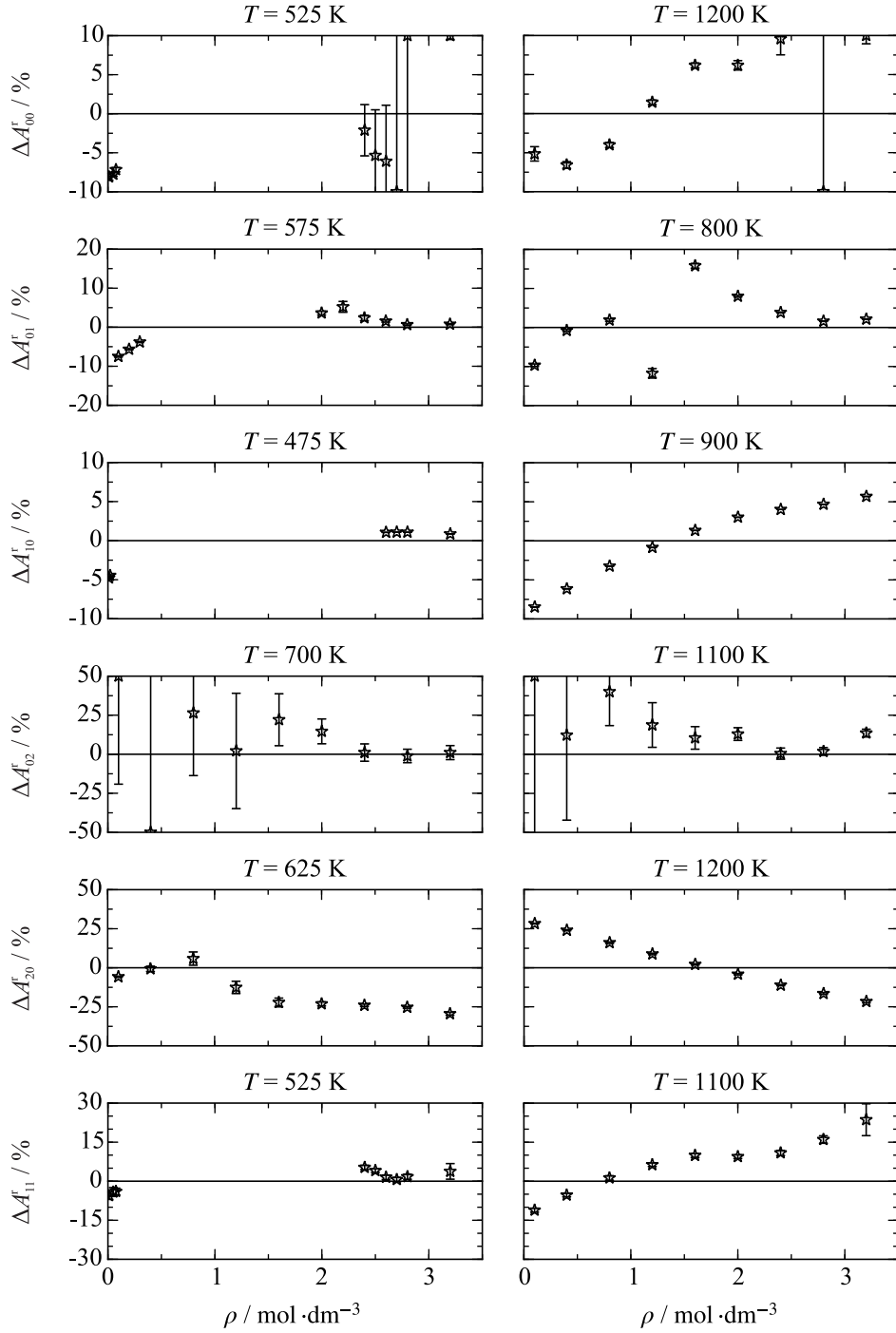


Figure 12. Relative deviations of simulated residual Helmholtz derivative data from the present equation of state along selected isotherms. Relative deviations are calculated according to Eq. (8).

Comparisons of the simulated residual Helmholtz derivatives from the present equation of state along selected isotherms are shown in Figure 12. A comprehensive overview about all available simulation data is given in the supplementary material. Deviations of the residual Helmholtz energy A_{00}^r and the first derivative with respect to the temperature A_{10}^r amount up to 10 %. Except for a few data points at the zero crossing or at very low densities, the same accuracy can be observed for the first derivative with respect to the density A_{01}^r . The first mixed derivative with respect to the temperature and density A_{11}^r is reproduced by the present

equation of state within 15 %. The second derivative with respect to the temperature A_{20}^r and the second derivative with respect to the density A_{02}^r differ by approximately 30 %. For a better classification of these deviations, the Helmholtz derivatives were transferred to common thermodynamic properties (pressure, heat capacities, and speed of sound) according to Eq. (12) and

$$p/(\rho RT) = 1 + A_{01}^r, \quad (13)$$

$$c_v/R = -(A_{20}^o + A_{20}^r), \text{ and} \quad (14)$$

$$c_p/R = -(A_{20}^o + A_{20}^r) + \frac{(1 + A_{01}^r - A_{11}^r)^2}{1 + 2A_{01}^r + A_{02}^r}. \quad (15)$$

For the calculation of caloric properties, the ideal contribution of the present equation of state was adopted.

In Figure 13, relative deviations of the common thermodynamic properties from the present equation of state are depicted. The homogeneous density and the isobaric heat capacity are represented within 2 %. The isochoric heat capacity differs from the present equation of state by 1 % and for $\rho \leq 1.2 \text{ mol}\cdot\text{dm}^{-3}$ the difference is even 0.5 %. Finally, the speed of sound data are reproduced within 7 %. Of course, for a reliable statement on the accuracy of the present equation of state, experimental measurements in this range are required.

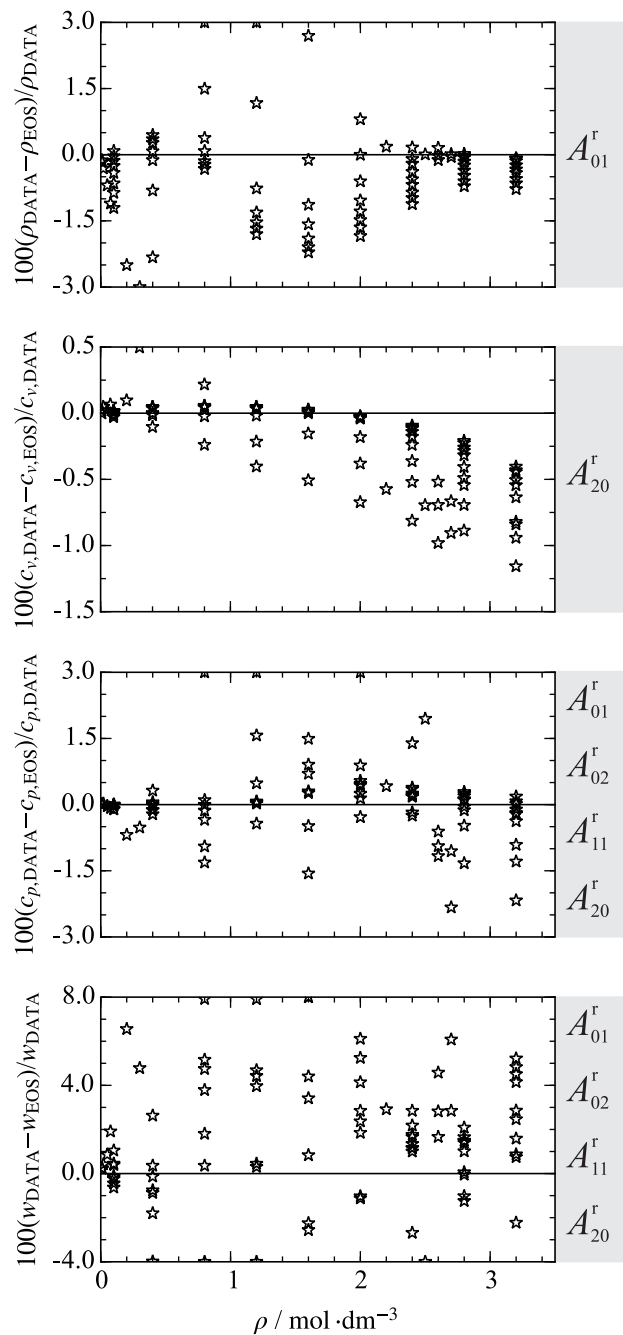


Figure 13. Comparison of the present equation of state with thermodynamic properties obtained from molecular simulation data generated in this work. The involved residual Helmholtz energy derivatives are indicated in the grey boxes.

5 PHYSICAL AND EXTRAPOLATION BEHAVIOR

In addition to the accurate representation of experimental and simulation data, the correct physical and extrapolation behavior in regions where no data are available is an essential aspect in the development of equations of state. Especially for the application to mixture models, a reasonable course of thermodynamic properties has to be ensured. Typical diagrams, which are analyzed during fitting procedures, are shown in Figure 14. On the top left, the vapor-liquid equilibrium is presented in a T - ρ diagram. The isobars are smooth and the rectilinear diameter is a straight line up to the critical point. The critical isobar exhibits a saddle point at the critical point. The hypothetical saturated liquid phase of the isochoric heat capacity (top right) increases with decreasing temperature, and both saturated phases merge at a maximum at the critical point. This diagram is also an indication for the qualitatively correct behavior of the speed of sound, which was observed during the fit as well. In the center of Figure 14, the phase identification parameter⁸⁶ is presented as function of density (left) and temperature (right). Both plots show a correct course as described by Thol *et al.*⁸⁷ and Lemmon *et al.*⁸⁸ No unreasonable changes in slope or curvature were observed. The virial coefficients B , C , and D are presented at the bottom (left). No unreasonable features can be observed for the second virial coefficient. The third virial coefficient exhibits a slight shift of its maximum to lower temperatures than the critical one. It should most likely be located closer to the critical temperature, similar to hexamethyldisiloxane.¹² Since this is not a fully investigated phenomenon and it is not experimentally proven that the maximum occurs approximately at the critical temperature, this slight shift was accepted here. The same holds for the fourth virial coefficient. The qualitative behavior is in very good agreement with the previously analyzed equations of state for the Lennard-Jones fluids^{87,89} and hexamethyldisiloxane.¹² However, the maximum is also not located at the critical temperature, but shifted to a lower value. A noticeable feature can be observed in the further course of the fourth virial coefficient. For the Lennard-Jones fluids,^{87,89} a second maximum was predicted from the equations of state and statistical mechanics independently. The same effect is observed here for octamethylcyclotetrasiloxane. Without any information on experimental virial coefficients, the present equation of state exhibits this second maximum. Finally, characteristic ideal curves⁹⁰ are presented on the bottom left of Figure 14. No unreasonable courses can be observed so that correct extrapolation behavior to very high temperatures, pressures, and densities is ensured.

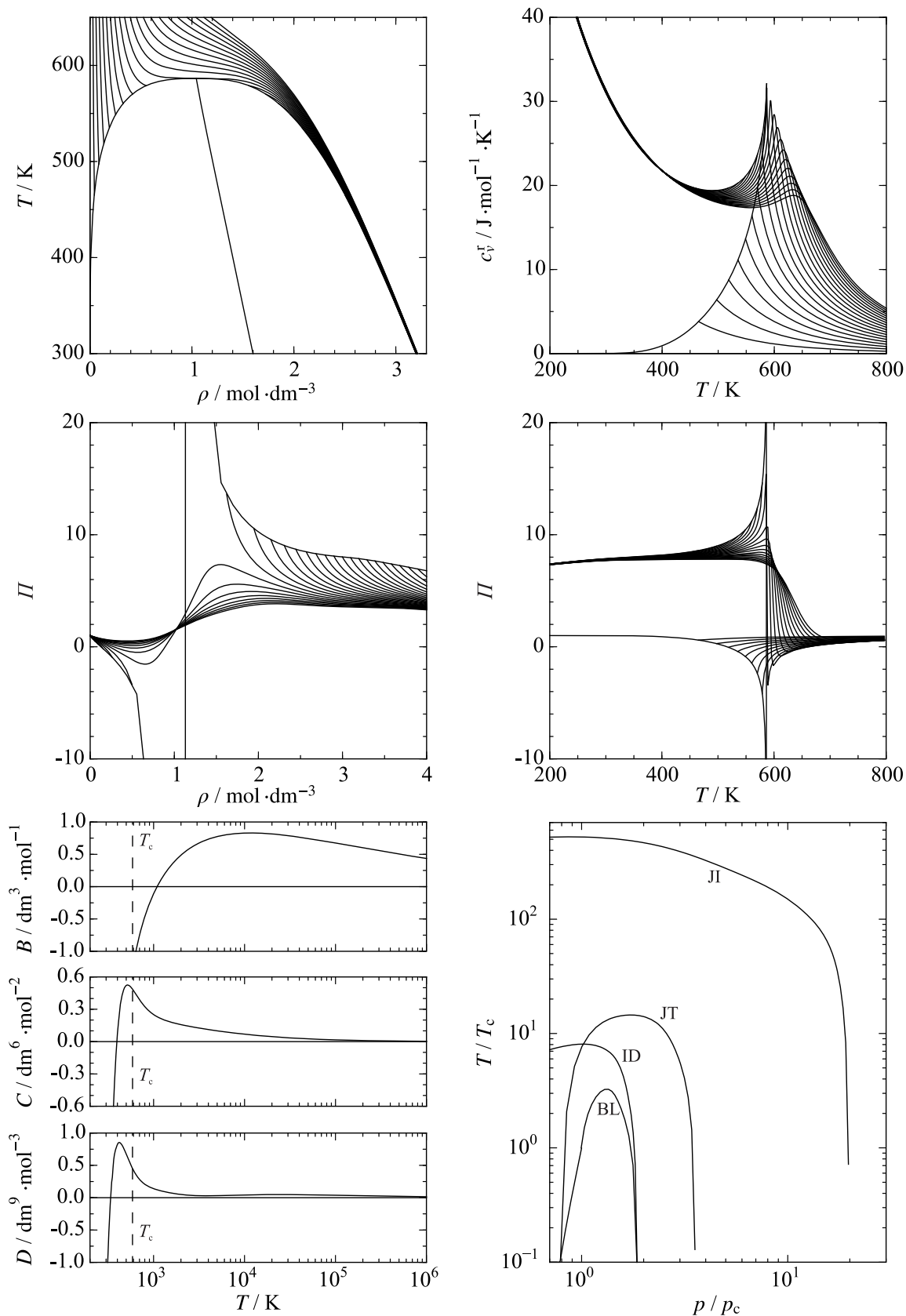


Figure 14. Plots of some thermodynamic properties of octamethylcyclotetrasiloxane: vapor-liquid equilibrium curves together with the rectilinear diameter (top left), residual isochoric heat capacity (top right), phase identification parameter as a function of temperature (center left), phase identification parameter as a function of density (center right), second, third, and fourth virial coefficients (bottom left), and characteristic ideal curves⁹⁰ (bottom right). ID: ideal curve, BL: Boyle curve, JT: Joule-Thomson inversion curve, JI: Joule inversion curve.

6 CONCLUSION

The present equation of state for octamethylcyclotetrasiloxane is written in terms of the reduced Helmholtz energy so that any equilibrium thermodynamic property can be obtained from its derivatives with respect to temperature and density. The ideal contribution contains three Planck-Einstein terms, whereas the residual contribution consists of five polynomial, five exponential, and five Gaussian bell-shaped terms. The range of validity based on experimental data is from the triple point to 590 K for pressures up to 180 MPa. The expected uncertainty of vapor pressure data from the present equation of state is 1.5 % for $T \leq 460$ K and 2 % for higher temperatures. Saturated liquid density data are accurate within 0.1 % for $T < 360$ K and 0.5 % for higher temperatures. The uncertainty of the homogeneous density at atmospheric pressure is assessed to be 0.1 %. The available experimental data in the high pressure region are not consistent with the present speed of sound measurements so that the equation is assumed to be accurate within only 0.7 %. The expected uncertainty of speed of sound data calculated with the present equation of state is 0.5 %. Next to the analysis of experimental measurements, the extrapolation behavior was investigated comprehensively and found to be reasonable. Finally, the range of validity was extended to $T_{\max} = 1200$ K and $p_{\max} = 520$ MPa by means of molecular simulation data. Since no experimental measurements are available in this region, no uncertainty statements can be made, but indications based on the simulation data are given.

Reference values to verify computer implementation are given in the supporting information. Additionally, ancillary equations were developed for the vapor pressure as well as saturated liquid and vapor densities, which can be used for initial calculations of starting values of iterative phase calculations. The corresponding equations and parameters are also listed in the supplementary material. Furthermore, a parameter file for the software packages TREND⁹¹ and REFPROP⁹² as well as a C++ source code are provided.

Acknowledgment

This work was part of a comprehensive research program supported by the German Research Foundation (DFG). The simulations were carried out on the national supercomputer hazelhen at the High Performance Computing Center Stuttgart (HLRS) within Project No. MMHBF2.

Supporting Information Available:

- Reference values to verify computer implementation.
- Ancillary equations for vapor pressure, saturated liquid density, and saturated vapor density.
- Parameter file for the software packages TREND⁹¹ and REFPROP⁹².
- C++ source code for the calculation of selected thermodynamic properties at homogeneous states.

This material is available free of charge via the Internet at <http://pubs.acs.org>.

7 REFERENCES

- (1) EPA National Center for Biotechnology Information, PubChem Compound Database; CID=11169. <https://pubchem.ncbi.nlm.nih.gov/compound/11169> (accessed November 3, 2015).
- (2) Colonna, P.; Nannan, N. R.; Guardone, A.; Lemmon, E. W., Multiparameter Equations of State for Selected Siloxanes. *Fluid Phase Equilib.* **2006**, *244*, 193–211.
- (3) Span, R.; Wagner, W., Equations of State for Technical Applications. I. Simultaneously Optimized Functional Forms for Nonpolar and Polar Fluids. *Int. J. Thermophys.* **2003**, *24*, 1–39.
- (4) Span, R.; Wagner, W., Equations of State for Technical Applications. II. Results for Nonpolar Fluids. *Int. J. Thermophys.* **2003**, *24*, 41–109.
- (5) Span, R.; Wagner, W., Equations of State for Technical Applications. III. Results for Polar Fluids. *Int. J. Thermophys.* **2003**, *24*, 111–162.
- (6) Thol, M.; Piazza, L.; Span, R., A New Functional Form for Equations of State for Some Weakly Associating Fluids. *Int. J. Thermophys.* **2014**, *35*, 783–811.
- (7) Sun, L.; Ely, J. F., A Corresponding States Model for Generalized Engineering Equations of State. *Int. J. Thermophys.* **2005**, *26*, 705–728.
- (8) Alexandrov, I.; Gerasimov, A.; Grigor'ev, B., Generalized Fundamental Equation of State for the Normal Alkanes (C5-C50). *Int. J. Thermophys.* **2013**, *34*, 1865–1905.
- (9) Grigor'ev, B.; Alexandrov, I.; Gerasimov, A., Generalized Equation of State for the Cyclic Hydrocarbons over a Temperature Range from the Triple Point to 700 K with Pressures up to 100 MPa. *Fluid Phase Equilib.* **2015**. DOI: 10.1016/j.fluid.2015.07.046.
- (10) Rutkai, G.; Thol, M.; Lustig, R.; Span, R.; Vrabec, J., Communication: Fundamental Equation of State Correlation with Hybrid Data Sets. *J. Chem. Phys.* **2013**, *139*, 041102.
- (11) Thol, M.; Rutkai, G.; Köster, A.; Kortmann, M.; Span, R.; Vrabec, J., Fundamental Equation of State for Ethylene Oxide Based on a Hybrid Dataset. *Chem. Eng. Sci.* **2015**, *121*, 87–99 and **2015**, *134*, 887–890.
- (12) Thol, M.; Dubberke, F.; Rutkai, G.; Windmann, T.; Köster, A.; Span, R.; Vrabec, J., Fundamental Equation of State Correlation for Hexamethyldisiloxane Based on Experimental and Molecular Simulation Data. *Fluid Phase Equilib.* **2015**. DOI: 10.1016/j.fluid.2015.09.047.
- (13) Lin, C.-W.; Trusler, J. P. M., The Speed of Sound and Derived Thermodynamic Properties of Pure Water at Temperatures Between (253 and 473) K and at Pressures up to 400 MPa. *J. Chem. Phys.* **2012**, *136*, 094511.

- (14) Dubberke, F. H.; Rasche, D. B.; Baumhögger, E.; Vrabec, J., Apparatus for the Measurement of the Speed of Sound of Ammonia up to High Temperatures and Pressures. *Rev. Sci. Instrum.* **2014**, *85*, 084901.
- (15) Ball, S. J.; Trusler, J. P. M., Speed of Sound of n-Hexane and n-Hexadecane at Temperatures Between 298 and 373 K and Pressures up to 100 MPa. *Int. J. Thermophys.* **2001**, *22*, 427–443.
- (16) Dubberke, F. H.; Baumhögger, E.; Vrabec, J., Burst Design and Signal Processing for the Speed of Sound Measurement of Fluids with the Pulse-echo Technique. *Rev. Sci. Instrum.* **2015**, *86*, 054903.
- (17) Gedanitz, H.; Davila, M. J.; Baumhögger, E.; Span, R., An Apparatus for the Determination of Speeds of Sound in Fluids. *J. Chem. Thermodyn.* **2010**, *42*, 478–483.
- (18) Harris, G. R., Review of Transient Field Theory for a Baffled Planar Piston. *J. Acoust. Soc. Am.* **1981**, *70*, 10–20.
- (19) Meier, K., The Pulse-echo Method for High Precision Measurements of the Speed of Sound in Fluids. Habilitation thesis, University of the Federal Armed Forces, Hamburg (Germany), 2006.
- (20) Glass, C. W.; Reiser, S.; Rutkai, G.; Deublein, S.; Köster, A.; Guevara-Carrion, G.; Wafai, A.; Horsch, M.; Bernreuther, M.; Windmann, T., ms2: A molecular Simulation Tool for Thermodynamic Properties, New Version Release. *Comp. Phys. Commun.* **2014**, *185*, 3302–3306.
- (21) Lustig, R., Direct Molecular NVT Simulation of the Isobaric Heat Capacity, Speed of Sound and Joule–Thomson Coefficient. *Mol. Sim.* **2011**, *37*, 457–465.
- (22) Lustig, R., Statistical Analogues for Fundamental Equation of State Derivatives. *Mol. Phys.* **2012**, *110*, 3041–3052.
- (23) Mohr, P. J.; Taylor, B. N.; Newell, D. B., CODATA Recommended Values of the Fundamental Physical Constants: 2010. *Rev. Mod. Phys.* **2012**, *84*, 1527–1605.
- (24) Span, R. *Multiparameter Equations of State: An Accurate Source of Thermodynamic Property Data*; Springer: Berlin, 2000.
- (25) Schmidt, M. W.; Baldridge, K. K.; Boatz, J. A.; Elbert, S. T.; Gordon, M. S.; Jensen, J. H.; Koseki, S.; Matsunaga, N.; Nguyen, K. A.; Su, S.; Windus, T. L.; Dupuis, M.; Montgomery, J. A., General Atomic and Molecular Electronic Structure System. *J. Comput. Chem.* **1993**, *14*, 1347–1363.
- (26) Merker, T.; Vrabec, J.; Hasse, H., Engineering Molecular Models: Efficient Parameterization Procedure and Cyclohexanol as Case Study. *Soft Mater.* **2012**, *10*, 3–24.

- (27) Matsubara, H.; Pichierri, F.; Kurihara, K., Design of a Versatile Force Field for the Large-Scale Molecular Simulation of Solid and Liquid OMCTS. *J. Chem. Theory Comput.* **2010**, *6*, 1334–1340.
- (28) Xu, R.-G.; Leng, Y., Solvation Force Simulations in Atomic Force Microscopy. *J. Chem. Phys.* **2014**, *140*, 214702.
- (29) Guevara-Carrion, G.; Nieto-Draghi, C.; Vrabec, J.; Hasse, H., Prediction of Transport Properties by Molecular Simulation: Methanol and Ethanol and their Mixture. *J. Phys. Chem. B* **2008**, *112*, 16664–16674.
- (30) Abbas, R.; Ihmels, E. C.; Enders, S.; Gmehling, J., Measurement of Transport Properties for Selected Siloxanes and their Mixtures Used as Working Fluids for Organic Rankine Cycles. *Ind. Eng. Chem. Res.* **2011**, *50*, 8756–8763.
- (31) Marsh, K. N., Mutual Diffusion in Octamethylcyclotetrasiloxane Mixtures. *Trans. Faraday Soc.* **1968**, *64*, 894.
- (32) Waterman, H. I.; Van Herwijnen, W. E. R.; Den Hartog, H. W., Statistical-Graphical Survey of Series of Linear and Cyclic Dimethylsiloxanes. *J. Appl. Chem.* **1958**, *8*, 625–631.
- (33) Reuther, H., Über Silikone XIV: Über das Viskosität-Temperatur-Verhalten von Silikonölen unter besonderer Berücksichtigung des Bereichs unter 0°C. *Chem. Tech.* **1953**, *5*, 268.
- (34) Wilcock, D. F., Vapor Pressure-Viscosity Relations in Methylpolysiloxanes. *J. Am. Chem. Soc.* **1946**, *68*, 691–696.
- (35) Rowley, R. L.; Wilding, W. V.; Oscarson, J.; Yang, Y.; Zuendel, N.; Daubert, T.; Danner, R. *DIPPR Data Compilation of Pure Chemical Properties*; Taylor & Francis Publishing Company: New York, 2004.
- (36) Haar, L.; Gallagher, J. S.; Kell, G. S., The Anatomy of the Thermodynamic Surface of Water: The Formulation and Comparisons with Data. *Sengers JV (ed.) Proc. 8th Symp. Thermophys. Prop., ASME, New York (1982)*; pp 298–302.
- (37) Setzmann, U.; Wagner, W., A New Equation of State and Tables of Thermodynamic Properties for Methane Covering the Range from the Melting Line to 625 K at Pressures up to 100 MPa. *J. Phys. Chem. Ref. Data* **1991**, *20*, 1061–1155.
- (38) Lemmon, E. W.; Jacobsen, R. T., A New Functional Form and New Fitting Techniques for Equations of State with Application to Pentafluoroethane (HFC-125). *J. Phys. Chem. Ref. Data* **2005**, *34*, 69–108.
- (39) Lemmon, E. W.; McLinden, M. O.; Wagner, W., Thermodynamic Properties of Propane. III. A Reference Equation of State for Temperatures from the Melting Line to 650 K and Pressures up to 1000 MPa. *J. Chem. Eng. Data* **2009**, *54*, 3141–3180.

- (40) Thol, M.; Lemmon, E. W.; Span, R., Equation of State for Benzene for Temperatures from the Melting Line up to 725 K with Pressures up to 500 MPa. *High Temp.-High Press.* **2012**, *41*, 81–97.
- (41) Zhou, Y.; Liu, J.; Penoncello, S. G.; Lemmon, E. W., An Equation of State for the Thermodynamic Properties of Cyclohexane. *J. Phys. Chem. Ref. Data* **2014**, *43*, 043105.
- (42) Young, C. L., Equilibrium Properties of Octamethylcyclotetrasiloxane near its Critical Point and Applicability of the Principle of Corresponding States. *J. Chem. Thermodyn.* **1972**, *4*, 65–75.
- (43) Mekhtiev, S. A.; Karasharli, K. A., Analysis of the Results of Thermodynamic Studies of a Series of Organosilicon Compounds. *Azerb. Khim. Zhur.* **1981**, *5*, 85–88.
- (44) Wieser, M. E.; Berglund, M., Atomic Weights of the Elements 2007 (IUPAC Technical Report). *Pure Appl. Chem.* **2009**, *81*, 2131–2156.
- (45) Frenkel, M.; Chirico, R. D.; Diky, V. Kroenlein, K.; Muzny, C. D.; Kazakov, A. F., Magge, J. W.; Abdulagatov, I. M.; Lemmon, E. W. *NIST Standard Reference Database 103b: NIST Thermo-Data-Engine - Pure Components, Binary Mixtures, Reactions, Version 8.0*; Standard Reference Data Program; National Institute of Standards and Technology: Gaithersburg, USA, 2013.
- (46) Harrison, B. K.; Seaton, W. H., Solution to Missing Group Problem for Estimation of Ideal Gas Heat Capacities. *Ind. Eng. Chem. Res.* **1988**, *27*, 1536–1540.
- (47) Nannan, N. R.; Colonna, P.; Tracy, C. M.; Rowley, R. L.; Hurly, J. J., Ideal-Gas Heat Capacities of Dimethylsiloxanes from Speed-of-Sound Measurements and ab initio Calculations. *Fluid Phase Equilib.* **2007**, *257*, 102–113.
- (48) Abbas, R.; Schedemann, A.; Ihmels, C.; Enders, S.; Gmehling, J., Measurement of Thermophysical Pure Component Properties for a Few Siloxanes Used as Working Fluids for Organic Rankine Cycles. *Ind. Eng. Chem. Res.* **2011**, *50*, 9748–9757.
- (49) Flaningam, O. L., Vapor Pressures of Poly(dimethylsiloxane) Oligomers. *J. Chem. Eng. Data* **1986**, *31*, 266–272.
- (50) Marsh, K. N., Thermodynamics of Octamethylcyclotetrasiloxane Mixtures. *Trans. Faraday Soc.* **1968**, *64*, 883–893.
- (51) Marsh, K. N., Enthalpies of Mixing and Excess Gibbs Free Energies of Mixtures of Octamethylcyclotetrasiloxane+Cyclopentane at 291.15, 298.15, and 308.15 K. *J. Chem. Thermodyn.* **1970**, *2*, 359–365.
- (52) Tomlins, R. P.; Marsh, K. N., A New Apparatus for Measuring the Vapour Pressure of Liquid Mixtures. Excess Gibbs Free Energy of Octamethylcyclotetrasiloxane + Cyclohexane at 308.15 K. *J. Chem. Thermodyn.* **1976**, *8*, 1185–1194.

- (53) Stull, D. R., Vapor Pressure of Pure Substances: Organic Compounds. *Ind. Eng. Chem.* **1947**, *39*, 517–540.
- (54) Hunter, M. J.; Hyde, J. F.; Warrick, E. L.; Fletcher, H. J., Organo-Silicon Polymers. The Cyclic Dimethyl Siloxanes. *J. Am. Chem. Soc.* **1946**, *68*, 667–672.
- (55) Patnode, W.; Wilcock, D. F., Methylpolysiloxanes. *J. Am. Chem. Soc.* **1946**, *68*, 358–363.
- (56) Korchemskaya, K. M.; Shakhparonov, M. I.; Lelchuk, S. L.; Korablina, T. P. Baburina, I. I.; Voronina, R. D., Pressure and Density of the Vapors of Binary Solutions of Chlorosilanes: IV. Silane. *Izv. Vyssh. Uchebn. Zaved., Khim. Khim. Tekhnol.* **1962**, *5*, 65–69.
- (57) Lopatkina, I. L.; Kucherskaya, L. A.; Kuznetsova, A. G.; Shaulov, Y. K., Vapour Pressure of Cyclosiloxanes. *Russ. J. Phys. Chem.* **1973**, *47*, 1626–1627.
- (58) Palczewska-Tulińska, M.; Oracz, P., Selected Physicochemical Properties of Hexamethylcyclotrisiloxane, Octamethylcyclotetrasiloxane, and Decamethylcyclopentasiloxane. *J. Chem. Eng. Data* **2005**, *50*, 1711–1719.
- (59) Palczewska-Tulińska, M.; Choliński, J.; Szafranski, A.; Wyrzykowska-Stankiewicz, D., Maximum-Likelihood Evaluation of Antoine Equation Constants for Vapor Pressures of Morpholine, n-Heptane, Cyclohexane and Methylcyclohexane. *Fluid Phase Equilib.* **1983**, *11*, 233–243.
- (60) Osthoff, R. C.; Grubb, W. T., Physical Properties of Organosilicon Compounds: III. Thermodynamic Properties of Octamethylcyclotetrasiloxane. *J. Am. Chem. Soc.* **1954**, *76*, 399–401.
- (61) Smith, A.; Menzies, A. W. C., Studies in Vapor Pressure. III. A Static Method for Determining the Vapor Pressures of Solids and Liquids. *J. Am. Chem. Soc.* **1910**, *32*, 1412–1434.
- (62) Ambrose, D.; Townsend, R., 681. Thermodynamic Properties of Organic Oxygen Compounds. Part IX. The Critical Properties and Vapour Pressures, above Five Atmospheres, of Six Aliphatic Alcohols. *J. Chem. Soc.* **1963**, *37*, 3614–3625.
- (63) Flaningam, O. L.; Williams, D. E., Octamethylcyclotetrasiloxane Azeotropes Patent No. US 5.492.647, May 8, 1995.
- (64) Hurd, C. B., Studies on Siloxanes: I. The Specific Volume and Viscosity in Relation to Temperature and Constitution. *J. Am. Chem. Soc.* **1946**, *68*, 364–370.
- (65) Weast, R. C.; Astle, M. J. *CRC Handbook of Data on Organic Compounds*; CRC Press: Boca Raton, Fla., 1985.
- (66) Golik, O. Z.; Cholpan, P. P. *Ukr. Fiz. Zh.* **1960**, *5*, 242–251.

- (67) Levien, B. J., Excess Volumes of Mixtures of Globular Molecules. II. *J. Chem. Thermodyn.* **1973**, *5*, 679–687.
- (68) McLure, I. A.; Barbarin-Castillo, J. M., Orthobaric Liquid Densities for Octamethylcyclotetrasiloxane, Decamethylcyclopentasiloxane, Dimethicone 20, and a Cyclic Poly(dimethylsiloxane). *J. Chem. Eng. Data* **1994**, *39*, 12–13.
- (69) Shinoda, K.; Hildebrand, J. H., Compressibilities and Iochores of $(C_3F_7COOCH_2)_4C$, $c-Si_4O_4(CH_3)_8$, $n-C_5H_{12}$, $n-C_8H_{18}$, $2,2,4-C_5H_9(CH_3)_3$, $c-C_5H_{10}$, $c-C_6H_{12}$, $c-C_6H_{11}CH_3$, $C_6H_5CH_3$, $p-C_6H_4(CH_3)_2$, $s-C_6H_3(CH_3)_3$, CH_2Cl_2 . *J. Phys. Chem.* **1961**, *65*, 183.
- (70) Tanaka, T., Heats of Formation of Lower Members of Dimethyl- and Methylisopropoxy-cyclopolysiloxanes. *Bull. Chem. Soc. Jpn.* **1960**, *33*, 282–286.
- (71) Schuh, H.-H.; Fischer, H., The Kinetics of the Bimolecular Self-Reaction of t-Butyl Radicals in Solution: I. Termination Rates. *Helv. Chim. Acta* **1978**, *61*, 2130–2164.
- (72) Herring, W.; Winnick, J., Excess Volumes of Octamethylcyclotetrasiloxane + Carbon Tetrachloride. *J. Chem. Thermodyn.* **1974**, *6*, 957–964.
- (73) Dickinson, E., Pressure Dependence of Shear Viscosity in n-Alkane + Dimethylsiloxane Mixtures. *J. Phys. Chem.* **1977**, *81*, 2108–2113.
- (74) Easteal, A. J.; Woolf, L. A., Self-diffusion and Volumetric Measurements for Octamethylcyclotetrasiloxane under Pressure at 323 K. *J. Chem. Soc. Faraday Trans. 1* **1984**, *80*, 549–551.
- (75) Mills, A. P.; MacKenzie, C. A., The Application of Bond Parachors to Organosilicon Chemistry. *J. Am. Chem. Soc.* **1954**, *76*, 2672–2673.
- (76) Myers, R. S.; Clever, H. L., Surface Tension of Octamethylcyclotetrasiloxane and Hexamethyldisilazane and their Solutions with Carbon Tetrachloride and n-Hexadecane. *J. Chem. Eng. Data* **1969**, *14*, 161–164.
- (77) Ross, M.; Hildebrand, J. H., Energy Volume Relations of Octamethylcyclotetrasiloxane and its Mixtures with Carbon Tetrachloride. *J. Phys. Chem.* **1963**, *67*, 1301–1303.
- (78) Wappmann, S. J.; Tarassov, I. N.; Lüdemann, H.-D., Densities of Octamethylcyclotetrasiloxane + Methane and 2,2-Dimethylpropane + Methane from 10 to 200 MPa and from 294 to 433 K. *J. Chem. Eng. Data* **1996**, *41*, 84–88.
- (79) Golik, A.; Cholpan, P. F., Investigation of Speed of Sound for Some Polysiloxanes. *Akusticheskij Zhurnal* **1961**, *7*, 33–39.
- (80) Niepmann, R.; Schmidt, U., Speeds of Sound in Liquid Octamethylcyclotetrasiloxane. *J. Chem. Thermodyn.* **1980**, *12*, 1133–1137.
- (81) Marsh, K. N.; Tomlins, R. P., Excess Enthalpies of Octamethylcyclotetrasiloxane Mixtures. *Trans. Faraday Soc.* **1970**, *66*, 783–790.

- (82) Wappmann, S. J.; Karger, N.; Lüdemann, H.-D., pVT Data of Liquid 1-, 2- and 3-Pentanol from 10 to 200 MPa and from 233 to 433 K. *J. Chem. Eng. Data* **1995**, *40*, 233–236.
- (83) Goodwin, R. D., Methanol Thermodynamic Properties from 176 to 673 K at Pressures to 700 Bar. *J. Phys. Chem. Ref. Data* **1987**, *16*, 799–892.
- (84) Back, P. J.; Easteal, A. J.; Hurle, R. L.; Woolf, L. A., High-precision Measurements with a Bellows Volumometer. *J. Phys. E: Sci. Instrum.* **1982**, *15*, 360–363.
- (85) Dubberke, F. H.; Riepold, M.; Baumhögger, E.; Vrabec, J., Speed of Sound of Oxygen in Supercritical States up to 500 K and 100 MPa. *J. Chem. Eng. Data* **2016**, *61*, 1632–1636.
- (86) Venkatarathnam, G.; Oellrich, L., Identification of the Phase of a Fluid Using Partial Derivatives of Pressure, Volume, and Temperature without Reference to Saturation Properties: Applications in Phase Equilibria Calculations. *Fluid Phase Equilib.* **2011**, *301*, 225–233.
- (87) Thol, M.; Rutkai, G.; Köster, A.; Span, R.; Vrabec, J.; Lustig, R., Equation of State for the Lennard-Jones Fluid. *accepted in J. Phys. Chem. Ref. Data* **2016**.
- (88) Lemmon, E. W.; Overhoff, U.; McLinden, M. O.; Wagner, W., Equation of State for Propylene **2016**, *to be published in J. Phys. Chem. Ref. Data*.
- (89) Thol, M.; Rutkai, G.; Span, R.; Vrabec, J.; Lustig, R., Equation of State for the Lennard-Jones Truncated and Shifted Model Fluid. *Int. J. Thermophys.* **2015**, *36*, 25–43.
- (90) Span, R.; Wagner, W., On the Extrapolation Behavior of Empirical Equations of State. *Int. J. Thermophys.* **1997**, *18*, 1415–1443.
- (91) Span, R.; Eckermann, T.; Herrig, S.; Hielscher, S.; Thol, M. *TREND. Thermodynamic Reference and Engineering Data 2.0*; private communication: Lehrstuhl für Thermodynamik, Ruhr-Universität Bochum: Bochum (Germany), 2015.
- (92) Lemmon, E. W.; Huber, M. L.; McLinden, M. O. *NIST Standard Reference Database 23: Reference Fluid Thermodynamic and Transport Properties-REFPROP, Version 9.1*; National Institute of Standards and Technology: Gaithersburg (USA), 2013.